University of Alberta

Polysiloxane Nanofibres via Surface Initiated Polymerization of Vapour Phase Reagents: Reaction Parameters, Mechanism of Formation and Wettability of the Fibre-bearing Substrates

by

De-ann Elaine Rollings ©

A thesis submitted to the Faculty of Graduate Studies and Research
in partial fulfillment of the requirements for the degree of

Master of Science

Chemistry

Edmonton, Alberta
Fall 2007

Library and Archives Canada

Published Heritage Branch

395 Wellington Street
Ottawa ON K1A 0N4
Canada

Bibliothèque et Archives Canada

Direction du Patrimoine de l'édition

395, rue Wellington
Ottawa ON K1A 0N4
Canada

Your file Votre référence
ISBN: 978-0-494-33335-8
Our file Notre référence
ISBN: 978-0-494-33335-8

NOTICE:
The author has granted a non-exclusive license allowing Library and Archives Canada to reproduce, publish, archive, preserve, conserve, communicate to the public by telecommunication or on the Internet, loan, distribute and sell theses worldwide, for commercial or non-commercial purposes, in microform, paper, electronic and/or any other formats.

The author retains copyright ownership and moral rights in this thesis. Neither the thesis nor substantial extracts from it may be printed or otherwise reproduced without the author's permission.

AVIS:
L'auteur a accordé une licence non exclusive permettant à la Bibliothèque et Archives Canada de reproduire, publier, archiver, sauvegarder, conserver, transmettre au public par télécommunication ou par l'Internet, prêter, distribuer et vendre des thèses partout dans le monde, à des fins commerciales ou autres, sur support microforme, papier, électronique et/ou autres formats.

L'auteur conserve la propriété du droit d'auteur et des droits moraux qui protège cette thèse. Ni la thèse ni des extraits substantiels de celle-ci ne doivent être imprimés ou autrement reproduits sans son autorisation.

In compliance with the Canadian Privacy Act some supporting forms may have been removed from this thesis.

While these forms may be included in the document page count, their removal does not represent any loss of content from the thesis.

Conformément à la loi canadienne sur la protection de la vie privée, quelques formulaires secondaires ont été enlevés de cette thèse.

Bien que ces formulaires aient inclus dans la pagination, il n'y aura aucun contenu manquant.

Canada

Abstract

Formation of high aspect ratio organosiloxane fibres of nano-dimensionality via surface induced vapour phase polymerization of vinyltrichlorosilane is described. First, the motivations of the presented work are outlined and put in perspective by providing background information on polysiloxanes, one dimensional materials, thin films, and superhydrophobic surfaces. Nanofibres of controlled dimensions, dispersion and density were fabricated on various hydroxylated substrates and characterized by XPS, EDX, SEM and variable angle FTIR. The critical parameters for fibre formation were isolated and a mechanism has been postulated based upon our findings from parameter iteration reactions. The aqueous wettability of fibre-bearing substrates was shown to be influenced by fibre spatial density and length. Superhydrophobic surfaces, $\theta_a > 150°$, were obtained using two different approaches: solution functionalization of calcined fibres with 3,3,3-trifluoropropyltrichlorosilane (FTS) and co-polymerization with FTS. A proof-of-concept patterning procedure is demonstrated by selected area growth of polysiloxane nanofibres. Finally, the general conclusions and future project objectives are outlined.

Acknowledgements

I would like to start off by thanking my supervisor, Jonathan Veinot without his guidance and support, I would not have been able to get this far. His patience with me, especially in the last few months, is commendable. He was also a great boss in that he always remembered that students have a life outside of graduate school, and encouraged us to live that life fully.

Next, I would like to thank my labmates: Janet Macdonald, Colin Hessel, Shaune McFarlane, Eric Henderson, Joel Kelly, José Rodríguez, Enrico Fok, and Bryan Rowsell. A special thanks goes to Colin (Coalin), Eric (Ricky), Joel (Jo-elly), and Shaune (Shaunie-boy) who have really been there for me through good times and bad. Thanks for always being there to pick me up or pick on me during the rough patches; both approaches usually brought on a smile. I'm extremely lucky to have these people as friends and will always look back with a laugh at the times we've had in grad school together.

With respect to my project, huge thanks are extended to Shufen Tsoi and George Braybrook. Shufen Tsoi initially discovered the polysiloxanes growing on substrates while she was trying to vapour functionalize her GLAD films. Without her inquisitive personality I would not have had a project to investigate. She also gave up a tremendous amount of time helping me collect SEM images as well as teaching me how to prepare samples and measure contact angles. George Braybrook spent countless hours with me imaging my substrates and always found extra time to fit my samples in when a deadline of mine was fast approaching.

I would also like to thank Jeremy Sit, a co-author on my first paper, and Mike Brett for his collaborations with our group.

Thanks to my roommates, Erin and Mike, for enduring a stress-filled, anxious roommate for the past few months. I greatly appreciate all the times you listened to me vent my frustrations as well as all of the words of encouragement that you gave me. I also appreciated the laughs I shared with you that helped to lighten my mood and brighten my spirits.

The university support staff was also incredibly helpful during my time here. Whether it be answering administration questions, or fabricating materials for me to conduct my research, someone was always willing to assist me.

Finally, I want to thank my friends and family. Their love, support and encouraging words gave me the extra boost I needed to complete my goals. I am forever indebted to my parents for everything that they have done for me. They taught me that hard work, determination and strong values are the keys to a achieving any goal or overcoming any obstacle faced. Words can't convey how grateful I am.

Table of Contents

Chapter 1: Introduction 1

1.1 Polysiloxane Nanofibres – An Overview 1

1.2 Polysiloxanes 2

1.2.1 Structural Characteristics Offering Unique Physical Properties 2

1.2.2 Common Polysiloxane Synthetic Procedures 4

1.3 Thin Films and Coatings 5

1.4 Self-Cleaning Surfaces 8

1.5 Advantages of One-Dimensional Polysiloxane Nanofibres 13

1.6 References 13

Chapter 2: Characterization and Preliminary Understanding of the Directed Growth Mechanism Resulting in Polysiloxane Nanofibres 16

2.1 Synthesis, Characterization of Polysiloxane Nanofibres and Mechanistic Aspects of their Formation. 17

2.2 References 26

Chapter 3: Apparatus Development 29

Chapter 4: Detailed analysis of the fibre forming process yielding polyvinylsiloxane nanofibres of tuneable dimensions and wettability 35

4.1 Parameter Variation 35

4.2 Mechanism of Formation 54

4.3 Tailored Wettability 63

4.4 Experimental Procedures 73

4.5 References 79

Chapter 5: Future Directions – Potential Functional Materials 35

5.1 Functionalization of currently prepared materials 81

5.1.1 Vinyl Group Functionalization 81

5.1.2 Functional Materials Accessible By Coupling to Surface Functionalities of the Polysiloxane Nanofibres 84

5.1.3 Poly(vinylsiloxane) as a precursor to Silicon Carbide 85

5.2 Modification of Si Precursor 88

5.2.1 $R_{4-x}SiCl_x$ 88

5.2.2 Variation of R, Si 89

5.3 Hierarchical Structure: Dry Adhesives 90

5.4 Conclusions 91

5.5 References 92

Appendices 99

List of Figures and Schemes

Figure 1-1. An illustration of the angle, (θ) formed by a water droplet at the substrate surface. 10

Figure 2-1. Oblique and side view SEM micrographs of a: **A.** high areal density, intertwined network of long fibres showing a ca. 400 nm packed layer. **B.** moderate areal density array of ca. 150 nm long fibres. **C.** low areal density, 100 nm fibres highlighting the uniformity of fibre diameters. 21

Figure 2-2. The influence of reagent structure on film morphology. Insets. Aqueous advancing contact angle measurements and reagent structures. **A.** HTS, **B.** 5-hexenyltrichlorosilane, **C.** VTMS, **D.** VTS. 22

Figure 3-1. Diagram of the apparatus currently being employed for the reaction conducted in Chapter 4. 32

Figure 3-2. Birdseye view of reaction chamber top. 33

Figure 4-1. SEM images of fibres obtained with (a) piranha cleaning, (b) sonication of substrate in increase polarity solvents: toluene, acetone, isopropyl alcohol, and water. Scale bars are 500 nm. 38

Figure 4-2. SEM (a) and AES mapping ((b) carbon, (c) oxygen, and (d) germanium) of an octyltrichlorosilane (OTS) functionalized oxide passivated Ge(100) wafer. Black regions in the SEM correspond to areas of high carbon and oxygen concentration in the AES analysis. This is consistent with large agglomerates of OTS. AES mapping color scale located to the right of the Ge

map; colours at the top of the colour bar correspond to higher intensity of the particular element in that region. Scale bars represent 500 nm. 41

Figure 4-3. SEM images of incompletely functionalized OTS SAM Ge wafers exposed to VTS. It is reasonable that areas where no fibre growth occurs are regions effectively functionalized by OTS. (a) high magnification image showing a single spot where no fibres formed, (b) low magnification image displaying the "holes" absent of fibres. Scale bars are 500 nm. 42

Figure 4-4. SEM images of fibres grown on substrates of varied composition and morphology, (a) SiO_2/Si(100) wafer, (b)GeO_2/Ge(100) wafer, (c) porous alumina, (d) high magnification of porous alumina showing fibres inside pores (e) 0.15 μm silica beads, (f) quartz, (g) capillary tube, (h) view of fibres located inside pore of capillary. Scale bars are 500 nm with the exception of images (g) and (h) where they represent 50 and 10 μm, respectively. 43

Figure 4-5. Oblique SEM images illustrating the influence of vinyltrichlorosilane volume on fibre formation: (a) 0.15 mL, (b) 0.25 mL, (c) 0.5 mL. Scale bars are 500 nm. 44

Figure 4-6. SEM micrographs showing the thin (<20 nm) and thick (~250 nm) polysiloxane films produced when (a) 40 μL (b) 60 μL of water was used. Scale bars are 0.5 and 5 μm, respectively. 48

Figure 4-7. Cross-sectional SEM images demonstrating the increased length (ℓ) of fibres with longer exposure times to VTS: (a) t_3 = 5 min, $\ell \sim 200$ nm, (b) t_3 = 10 min, $\ell \sim 500$ nm, (c) $t_3 > 20$ min, $\ell \sim 1.1$ μm. Scale bars are 500 nm. 51

Figure 4-8. A survey XP spectrum of VTS/FTS co-polymer fibres displaying the peaks corresponding to Si, C, O, and F. Inset, high-resolution spectrum of the carbon 1s region. The higher energy peak observed in the C 1s high-resolution spectrum is due to fluorine atoms bonded to the third carbon of the propyl group on 3,3,3-trifluoropropylsilane. SEM of the co-polymer fibres. Scale bar is 500 nm. 53

Figure 4-9. (a) Cartoon depicting the PDMS stamping process used to pattern the Si wafer. Left side of Si substrate stamped with 3,3,3-fluoropropyltrichlorosilane (FTS) before exposure to VTS. (b) SEM image showing a successfully patterned region of the Si wafer. Nanofibres preferentially grow an areas of the substrate not stamped with FTS. Scale bar is 50 μm. 61

Figure 4-10. X-ray photoelectron spectrum (left) and SEM image (right) of nanofibres calcined at 500°C that were subsequently solution functionalized with 3,3,3-fluoropropyltrichlorosilane. Scale bar is 500 nm. 62

Figure 4-11. SEM images and corresponding contact angles demonstrating the effect of fibre length and spatial dispersion on wettability of the substrate: (a) moderately disperses fibres ~200 nm in height, (b) sparsely distributed fibres ~100 nm in height, (c) densely packed fibres ~1 μm in height. Scale bars are 500 nm. 66

Figure 4-12. A stream of water rebounding off the surface of a Si wafer bearing co-polymer fibres of VTS/FTS. The reflection of the stream and water droplets is observed on the wafer. 68

Figure 5-1. Traditional organic reaction pathways accessible with olefin groups. Details of the reactions can be found elsewhere. [1] 82

Figure 5-2. Representative organic transformation available for 1° alcohol obtained through the electrophilic addition to an olefin .[1] 83

Figure 5-3. Various reaction pathways available with an aldehyde.[1] 84

List of Tables

Table 4-1. A summary of the influence water/ silane volumes and time intervals have on the fibre structures produced. Descriptions of the surface structures are assessed by SEM. Reaction conditions affording fibres as described in Entry 1 are adopted as the standard reaction conditions. 45

Chapter 1: Introduction

1.1 Polysiloxane Nanofibres – An Overview

The work presented in this thesis is centred on the fabrication of one-dimensional polysiloxane nanofibres by surface induced polymerization of vapour phase reagents. More specifically, reaction parameters are identified and the influence of each parameter on the growth of nanofibres is addressed. The knowledge gained from the presented reaction parameter investigations is then used to develop a mechanism for the fibre-forming process. Finally, the findings from studies on the aqueous wetting behaviour of fibre-bearing substrates are presented.

Our interest in fabrication of polysiloxane nanofibres is illustrated by summarizing the many unique and useful properties that polysiloxanes possess. In addition, previous work conducted on thin films and coatings as well as superhydrophobic surfaces is reviewed because the nanofibres examined herein alter the surface chemistry and properties of the substrate they are grown on. It is our hope that by presenting the background knowledge in these fields of research that the reader will more clearly see the how the work presented in thesis contributes to these fields of study.

1.2 Polysiloxanes

1.2.1 Structural Characteristics Offering Unique Physical Properties

Many of the interesting properties associated with siloxane polymers stem from their molecular structure, a Si-O backbone and organic pendant chains. The remarkable pliability as well as the chemical, thermal and physiological stability of polysiloxanes arise from the Si-O bonding, whereas properties such as low surface tension and substrate adhesion are imparted by the organic pendant groups.[1] Comparing a siloxane and carbon chain, one sees that the bond length and angle of the Si-O-Si bond is longer (1.64 Å) and wider (143°) than a chain of 3 carbons (1.53 A, 109°).[2] The angle of the Si-O-Si bond is also variable with the capability of passing through a linear 180° state[2]. As a result of the extended bond length and more obtuse bond angle, intra-molecular congestion around the skeletal chain is minimized thus increasing the rotation capability of the chains. Chain mobility is further increased by oxygen atoms in the Si-O backbone not having any substituents to hinder rotation around the skeletal backbone. Siloxane chains may also orient themselves in very unusual conformations due to the variability of the Si-O-Si bond angle and the dramatic difference in the sizes of the silicon and oxygen atoms.[2] These unique characteristics impart polysiloxanes with low glass transition temperatures. That is, polysiloxanes can withstand much lower temperatures than many organic polymers before becoming brittle.

The surface energy of solid polysiloxanes and surface tension of liquid polysiloxanes are dictated by the organic pendant groups; hydrophilic side chains increase the surface tension of the resulting polymer where as hydrophobic side chains decrease the surface tension. For this reason, vinylpolysiloxane is hydrophobic. Organic functionalities also affect the rotational and conformal flexibility of the siloxane chain ultimately influencing the glass transition and melting temperatures as well as the elastic modulus of the polymer.[1] In this manner, the extensive variability of the physical properties of siloxanes and their corresponding polymer chains is owed to pendant organic moieties. That is, the physical properties of polysiloxanes can be tailored to provide materials with specific physical properties (*vide infra*).

Co-polymerization is yet another strategy used to design polysiloxanes with desired physical characteristics.[3] Three practices are commonly adopted: co-polymerization of silicon-based monomers having different substituents, co-polymerization of silicon-based and purely carbon based monomers, and finally, graft polymerization of another polymer to the pendant chain of the siloxane or the reverse.[2,3] With all three approaches in hand, polysiloxanes offer outstanding adaptability with respect to the physical properties of the resulting material.

The intrinsic tuneability of polysiloxanes via introduction of pendant organic functionalities and numerous co-polymerization approaches have afforded their use in many seemly contradictory applications. For example, polysiloxanes have found use as both foam stabilizers as well as anti-foaming agents, mould-

releasing agents and pressure adhesives. Polysiloxanes have also found use as lubricants, chromatographic columns, protective coatings, water repellent sealants, cooking utensils, soft lithography, biomedical devices and elastomeric materials manufactured for harsh elements because of the high thermal and chemical stabilities, low toxicity, elasticity and high gas permeability of these materials.[2]

1.2.2 Common Polysiloxane Synthetic Procedures

Common methods for the synthesis of polysiloxanes include hydrolysis of alkylchlorosilanes, ring opening polymerization, living radical polymerization, and metal catalyzed polymerization. Polysiloxane thin films and coatings are generally fabricated by plasma polymerization, UV curable liquid polysiloxanes, and glow discharge. [4]

The synthesis of polysiloxane fibres of any length scale is fairly uncommon; however, two other research groups have published reports on the synthesis of polysiloxane nanofibres. Both groups fabricated poly(methylsiloxane) nanofibres using two different methods. The first procedure employed a solution-based polymerization of methyltrichlorosilane in the presence of trace water in toluene.[5,6] Phase separation occurs when toluene swollen polysiloxane fibres are extracted with ethanol. The fibres produced have diameters of approximately 40 nm and lengths >50 nm. Poly(methylsiloxane) fibres were also formed on various substrates by the hydrolysis of vapour phased methyltrichlorosilane in a controlled humidity reactor at atmospheric pressure. Fibres formed by this technique are typically 20 - 50 nm in diameter and have a

wide range of lengths up to 1 μm. Less frequently, fibres with 150 nm diameter and several microns long are produced with this procedure.

Both research groups focus on the development of hydrophobic surfaces and study the aqueous wettability of the resulting fibre modified substrates. Their primary interest in the poly(methylsiloxane) fibres stems from the excellent water repellency that these fibres exhibit. Gao *et al.*, have used these fibres to develop a new method for quantifying the extreme hydrophobicity and Zimmerman *et al.*, investigated polymethylsiloxane nanofibres for their suitability as outdoor self-cleaning surfaces by evaluating their weather durability. Neither group has commented on the factors that affect fibre formation or presented any mechanism outlining the process of formation. The work presented in Chapter 4 addresses these issues.

1.3 Thin Films and Coatings

Thin films and coatings are desirable for their ability to modify the reactivity/properties of surfaces without compromising the structural integrity of the bulk solid. For example, thin films are used to prevent corrosion, promote adhesion, alter the wettability, prevent contamination, lubricate or make a substrate biocompatible/bioactive.[7,8] Due to their extensive application across a broad range of industries, many different types of coatings and procedures have been developed including polymer grafting, Langmuir-Blodgett films, and self-assembled monolayers.

Langmuir-Blodgett films were among the first well-defined "molecular-scale" layers assembled on surfaces.[9] These layers are formed by transferring amphiphilic molecules such as fatty acids that organize at the surface of a liquid onto a solid surface by controlled immersion and emersion of the solid from the liquid. Well-packed layers are formed on the substrate surface when amphiphilic molecules present at the water/vapour interface are forced to assemble into a closely packed monolayer by pressure application perpendicular to the interface before and during transfer of the amphiphilic molecules.[9] This method provides mono or multi-layers adsorbed to a substrate surface. Langmuir-Blodgett layers are not robust as there is no link to the substrate surface.

Self-assembled monolayers are made up of molecules that have a long aliphatic chain and a head group that has a high affinity for the substrate. These molecules organize on a substrate to form a densely packed monolayer. Alkylthiols and alkylsilanes are two types of bi-functional molecules commonly used for SAMs. Thiols have the tendency to adsorb strongly on gold due to the strong soft/soft interactions and for this reason, SAMs of alkylthiols are typically fabricated on gold substrates or thin films.[10-12] Alkylsilanes on the other hand have been assembled on numerous substrates including gold[13] and mica,[14,15] but are predominately formed on hydroxyl terminated surfaces.[16-20] Alkylsiloxane monolayers are typically formed by solution or vapour phase methods using alkyltrichloro- or alkyltrialkoxysilanes as the amphiphilic reagent. In each case, a small quantity of water localized at the substrate surface hydrolyses the reagent,

resulting in the formation of alkyltrihydroxylsilane. Ordered layers of molecules self-assemble on the substrate surface because of the van der Waal's interactions between the alkyl chains, the high affinity of the silanol head groups for the substrate, and the irreversible condensation reactions that takes place between silanol head groups and the terminal hydroxyl groups on the substrate. These monolayers are significantly more robust than thiol SAMs or Langmuir-Blodgett films due to covalent bonds that are formed between the organosilanes and the substrate. Despite widespread study, siloxane SAMs are still plagued with reproducibility issues arising from the difficulties associated with controlling low water content in the solvent. There is also tremendous discrepancy in the literature concerning the synthetic procedures for producing densely packed monolayers.[14,16,17,20-25]

Polymer grafting is yet another method used to place a thin film or coating that is covalently bonded onto a surface. When polymer chains are grafted to the surface with a high density, chains form well-packed layers that are commonly referred to as polymer brushes. The grafting procedure is accomplished in two ways: 'grafting to' and 'grafting from' the surface. 'Grafting to' methods involve coupling end-functionalized polymers to a substrate surface. Conversely, for 'grafting from' procedures, initiator species present on the surface induce monomer polymerization. Polymer brush coatings exhibit excellent chemical and mechanical stability[26] as well as tuneable density, thickness and end-functionality. Polymer brushes grafted from substrates by surface initiated polymerization are

usually more densely packed than those fabricated by grafting to methods as a result of the steric hindrance imposed by already grafted chains. However, the fabrication of polymer brushes quite often requires that a catalyst be functionalized to the surface prior to polymerization.

The method presented in this work provides a route to introducing a high surface area fibrous mat onto a substrate without the use of a catalyst.

1.4 Self-Cleaning Surfaces

The lotus leaf is nature's self-cleaning surface. Droplets of water that fall onto the leaf bead on the surface and do not easily come to rest. Instead, they stay in motion, rolling on the surface, picking up dirt as they move. Finally, the drop rolls off the leaf taking any dirt from the surface with it when it leaves. A German botanist, Barthlott, was the first to suggest a reason for this unique behaviour based on a study of the microscopic structure of various plant leaves. He observed that plants leaves similar to those found on the lotus possessed a regular hierarchical structure of nano-scale roughness superimposed on micro sized wax crystalloid structures.[27] Although the connection between surface roughness and water repellency has been established,[18,28] the link between water repellency and contaminant removal had not. Decreased contact area, and therefore interaction between a water droplet and a rough surface has proven to be the reason behind both behaviours. When a drop is placed on the surface, an interface is formed between the three phases: air, liquid, and solid. The ability of the liquid to wet the

surface depends on the relative energies of the air-liquid, liquid-solid, and solid-air interfaces. The liquid either wets or repels the surface. For water on a hydrophobic surface, the liquid-solid interface is higher in energy then the liquid-air interface. As a result, the lowest energy state is satisfied by water forming a bead. If the hydrophobic surface also has nano/microscopic scale roughness, the water bead rests on top of the features rather than conforming to the roughness. That is, the droplet rests on a composite air/solid surface. In this manner, the interaction between the solid and the liquid is further reduced while the air-liquid interaction is maximized.

If solid contaminants are on a surface with roughness of smaller scale than the particulate, the solids are unable to conform to the surface. That is, the roughness of the underlying surface decreases the interaction between the particle and said solid by decreasing the contact area. As a result, the surface adhesion of the contaminant is decreased. When a water droplet comes in contact with the contaminant particle, the potential exists for a greater interaction with the drop,[27] and the particle is removed when the droplet rolls off the leaf. This unique behaviour was coined "the lotus effect" by Barthlott, and his work the impetus for designing hydrophobic hierarchically structured surfaces as artificial self-cleaning surfaces.

Prior to outlining methods currently available for fabricating superhydrophobic surfaces, it is useful to examine the common procedures and terminology used to evaluate the behaviour of liquid droplets on a surface. The

widely accepted method for evaluating the self-cleaning nature of substrates is the contact angle of water on the substrate (Figure 1-1). Two standard contact angles are measured: advancing and receding. The advancing contact angle is acquired by dispensing a drop of water on the surface then increasing the volume of the drop by the addition of more water. The receding angle is defined as the angle exhibited by the drop after a portion of the drop's volume has been removed. Contact angle hysteresis is the difference between the advancing and receding angles. Surfaces displaying advancing contact angles > 150° are deemed superhydrophobic, a term traditionally synonymous with "the lotus effect". However, many manufactured superhydrophobic surfaces are not self-cleaning due to their low receding angles, *i.e.*, the water droplet sticks to the surface. For this reason, researchers have begun using the contact angle hysteresis in combination with the advancing contact angle to describe the wetting nature of the surface. Those surfaces exhibiting self-cleaning behaviour are represented by a low contact angle hysteresis and a high advancing angle.

Figure 1-1. An illustration of the angle, (θ) formed by a water droplet at the substrate surface.

Currently, there are two primary strategies adopted for the production of superhydrophobic surfaces: 1. introducing rough surface topography on low energy materials or, 2. fabricating rough structures and subsequently functionalizing these structures with a hydrophobic substance. Additionally, it is useful to note that superhydrophobicity and the self-cleaning behaviour have been observed on both regular and irregular geometries. Methods for creating superhydrophobic surfaces with random geometries include: electroless galvanic deposition,[29] *in-situ* hydrothermal synthesis,[30] electrochemical etching/wet chemical etching,[31] electrospinning,[32] plasma fluorination of a polymeric surface,[33] melt solidification of alkylketene dimers,[34] metal salt crystallization,[35] and alkyltrialkoxysilane sol-gel foams.[36] Regular geometries are most commonly fabricated using lithographic techniques[37-40] however hydrothermal synthesis, glancing angle deposition,[8,41] and templates such as porous alumina discs[42] and polystyrene beads[43] have also been employed.

The advantage of regular geometrical roughness is it enables the direct study of dimensions/length scale required to realize superhydrophobicity. In one such study, McCarthy determined that hexagonal arrays of square pillars with dimension, x, and spacing, 2x, needed $x < 32$ μm if superhydrophobicity was to be observed. The hysteresis between the advancing and receding for these arrays remained very large, $\Delta\theta > 30°$; however, it was found that this could be decreased by changing the shape of the posts.[40] Extrand extended this work to include regular asperities with sloped tops, and developed a empirical model to predict the

correct geometry needed to obtain superhydrophobic surfaces.[39] In addition, the impact of hierarchical structuring on the receding angle was investigated experimentally recently by McCarthy *et al*. It was shown that hydrophobized, staggered posts exhibited an increase in the receding angle from 156° to 176° upon inclusion of a nano-scaled fibrous polymer.[6] A mathematical model was also developed by Patankar[44] that illustrated the importance of hierarchical structure when using pillar geometries. To this end, mathematical relationships have been derived to predict the contact angles of various structured surfaces. Two different approaches have been taken in this regard; one method considers the contact area between the drop and the surface and the other is based on the interactions occurring at the three phase contact line encompassing the drop. A detailed discussion of the two theories with application to the polysiloxane nanofibres fabricated in this work is presented in Chapter 4.

Many of the current techniques used for fabricating self-cleaning surfaces suffer from expensive lithographic techniques or other labour-intensive procedures. In addition, the materials prepared often lack the mechanical stability required for many applications. In order for artificial self-cleaning surfaces to become practical, economic, technically simple methods that produce mechanically stable structures are needed.

1.5 Advantages of One-Dimensional Polysiloxane Nanofibres

The polysiloxane fibres have the potential of providing a straightforward method for altering the chemistry of substrate surfaces while also introducing high surface area and high aspect ratio fibres. Additionally, the method presented in this thesis is conducted in the vapour phase, uses no solvents and as a result may be viewed as a more economical and environmentally friendly alternative. The ability to tune the mechanical properties of polysiloxanes also makes them highly valuable materials when mimicking natural phenomena. A more detailed discussion is presented in Chapter 5.

1.6 References

1. *Silicon-Based Polymer Sicence A Comprehensive Resource*; Zeigler, J. M.; Fearon, G. F. W., Eds.; American Chemical Society: Washington, DC, 1990.
2. Mark, J. E.; Allcock, H. R.; West, R. *Inorganic Polymers*; 2nd ed.; Oxford University Press: New York, 2005.
3. *Synthesis and Properties of Silicones and Silicone-Modified Materials*; Clarson, S. J.; Fitzgerald, J. J.; Owen, M. J.; Smith, S. D.; Van Dyke, M. E., Eds.; American Chemical Society: Washington, DC, 2003.
4. Bausch, G. G.; Stasser, J. L.; Tonge, J. S.; Owen, M. J. *Plasmas Polym.* **1998**, *3*, 23-34.
5. Gao, L.; McCarthy, T. J. *Langmuir* **2006**, *2006*, 2966-2967.
6. Gao, L.; McCarthy, T. J. *J. Am. Chem. Soc.* **2006**, *128*, 9052-9053.
7. Kim, H. W.; Chung, C. W.; Rhee, Y. H. *Int. J. Biol. Macromol.* **2005**, *35*, 47-53.
8. Tsoi, S.; Fok, E.; Sit, J. C.; Veinot, J. G. C. *Langmuir* **2004**, *20*, 10771-10774.
9. Blodgett, K. B. *J. Am. Chem. Soc.* **1934**, *56*, 495-495.
10. Nuzzo, R. G.; Allara, D. L. *J. Am. Chem. Soc.* **1983**, *105*, 4481-4483.
11. Porter, M. D.; Bright, T. B.; Allara, D. L.; Chidsey, C. E. D. *J. Am. Chem. Soc.* **1987**, *109*, 3559-3568.
12. Troughton, E. B.; Bain, C. D.; Whitesides, G. M.; Nuzzo, R. G.; Allara, D. L.; Porter, M. D. *Langmuir* **1988**, *4*, 365-385.

13. Finklea, H. O.; Robinson, L. R.; Blackburn, A.; Richter, B.; Allara, D.; Bright, T. *Langmuir* **1986**, *2*, 239-244.
14. Kessel, C. R.; Granick, S. *Langmuir* **1991**, *7*, 532-538.
15. Carson, G.; Granick, S. *J. Appl. Polym. Sci.* **1989**, *37*, 2767-2772.
16. Sagiv, J. *J. Am. Chem. Soc.* **1980**, *102*, 92-98.
17. Wasserman, S. R.; Tao, Y. T.; Whitesides, G. M. *Langmuir* **1989**, *5*, 1074-1087.
18. Wenzel, R., N. *Ind. Eng. Chem.* **1936**, *28*, 988-994.
19. Hoffmann, P. W.; Stelzle, M.; Rabolt, J. F. *Langmuir* **1997**, *13*, 1877-1880.
20. Onclin, S.; Ravoo, B. J.; Reinhoudt, D. N. *Angew. Chem. Int. Ed.* **2005**, *44*, 6282-6304.
21. McGovern, M. E.; Kallury, K. M. R.; Thompson, M. *Langmuir* **1994**, *10*, 3607-3614.
22. Le Grange, J. D.; Markham, J. L.; Kurkjian, C. R. *Langmuir* **1993**, *9*, 1749-1753.
23. Silberzan, P.; Leger, L.; Ausserre, D.; Benattar, J. J. *Langmuir* **1991**, *7*, 1647-1651.
24. Bierbaum, K.; Grunze, M.; Baski, A. A.; Chi, L. F.; Schrepp, W.; Fuchs, H. *Langmuir* **1995**, *11*, 2143-2150.
25. Bunker, B. C.; Carpick, R. W.; Assink, R. A.; Thomas, M. L.; Hankins, M. G.; Voigt, J. A.; Sipola, D.; De Boer, M. P.; Gulley, G. L. *Langmuir* **2000**, *16*, 7742-7751.
26. Edmondson, S.; Osborne, V. L.; Huch, W. T. S. *Chem. Soc. Rev.* **2004**, *33*, 14-22.
27. Barthlott, W.; Neinhuis, C. *Planta* **1997**, *202*, 1-8.
28. Cassie, A. B. D.; Baxter, S. *Trans. Faraday. Soc.* **1944**, *40*, 546-551.
29. Larmour, I. A.; Bell, S. E. J.; Saunders, G. C. *Angew. Chem. Int. Ed.* **2007**, *46*, 1710-1712.
30. Shi, F.; Chen, X.; Wang, L.; Niu, J.; Yu, J.; Wang, Z.; Zhang, X. *Chem. Mater.* **2005**, *17*, 6177-6180.
31. Wang, M. F.; Raghunathan, N.; Ziaie, B. *Langmuir* **2007**, *23*, 2300-2303.
32. Ma, M.; Hill, R. M.; Lowery, J. L.; Fridrikh, S. V.; Rutledge, G. C. *Langmuir* **2005**, *21*, 5549-5554.
33. Woodward, I.; Schofield, W. C. E.; Roucoules, V.; Badya, J. P. S. *Langmuir* **2003**, *19*, 3432-3438.
34. Shibuichi, S.; Onda, T.; Satoh, N.; Tsujii, K. *J. Phys. Chem.* **1996**, *100*, 19512-19517.
35. Guo, Z.-G.; Fang, J.; Hao, J.-c.; Liang, Y.-m.; Liu, W.-m. *ChemPhysChem* **2006**, *7*, 1674-1677.
36. Shirtcliffe, N. J.; McHale, G.; Newton, M. I.; Perry, C. C.; Pyatt, F. B. *Appl. Phys. Lett.* **2006**, *89*, 104106-2.
37. Zhu, L.; Feng, Y.; Ye, X.; Zhou, Z. *Sensors and Actuators, A: Physical* **2006**, *130-131*, 595-600.

38. Martines, E.; Seunarine, K.; Morgan, H.; Gadegaard, N.; Wilkinson, C. D. W.; Riehle, M. O. *Nano Letters* **2005**, *5*, 2097-2103.
39. Extrand, C. W. *Langmuir* **2002**, *18*, 7991-7999.
40. Öner, D.; McCarthy, T. J. *Langmuir* **2000**, *16*, 7777-7782.
41. Tsoi, S.; Fok, E.; Sit, J. C.; Veinot, J. G. C. *Chem. Mater.* **2006**, *18*, 5260-5266.
42. Xu, J.; Li, M.; Zhao, Y.; Lu, Q. *Colloids and Surfaces A: Physicochemical and Engineering Aspects* **2007**, *302*, 136-140.
43. Li, Y.; Cai, W.; Cao, B.; Duan, G.; Sun, F.; Li, C.; Jia, L. *Nanotechnology* **2006**, *17*, 238-243.
44. Patankar, N. A. *Langmuir* **2004**, *20*, 8209-8213.

Chapter 2: Characterization and Preliminary Understanding of the Directed Growth Mechanism Resulting in Polysiloxane Nanofibres

All experiments discussed in the following chapter were conducted by the author of this thesis. Polysiloxane nanofibre growth on Si wafers was initially observed by Shufen Tsoi (Electrical Engineering) while attempting vapour phase self-assembled monolayer (SAM) formation of vinyltrichlorosilane on a Si wafer for a collaborative project of the Veinot and Sit research groups. Modifications of the vapour phase SAM fabrication procedure and experimental equipment were required to obtain the results presented herein; these modifications were carried out by me with guidance and suggestions by Jonathan Veinot. All authors: De-ann Rollings, Shufen Tsoi, Jeremy Sit, and Jonathan Veinot contributed to discussions regarding the mechanism of formation. The following chapter is a direct reproduction of the communication that appeared in Langmuir and was written by me (*i.e.*, D. Rollings) with editorial suggestions from Jonathan Veinot. Permission to use the report in this thesis has been granted by the co-authors.

Reproduced with permission from *Langmuir*, **2007,** 23, 5275-5278. Copyright 2007 American Chemical Society.

2.1 Synthesis, Characterization of Polysiloxane Nanofibres and Mechanistic Aspects of their Formation.

One-dimensional (1D) materials such as nanofibres are the subject of fundamental and technological interest because of their unique properties arising from high aspect ratios, large surface areas, as well as their optical and electronic response. Notable devices that incorporate 1-D materials include ultraviolet lasers,[1] optical switches,[2] field effect transistors,[3] diodes,[4] and sensors.[3,5-7] More specifically, silicon oxide nanofibres have demonstrated device application as emissive materials, in nanoelectronics and in integrated optical devices. Examples of such applications include: low dimensional waveguides for functional microphotonics, scanning near field optical microscopy, optical interconnects on optical microchips, biosensors, and optical transmission antennae. [8-11] It is reasonable that by incorporating organic functionalities to form organosiloxane nanofibres, the physical properties of the fibres may be tailored to the fit application requirements (*e.g.*, elasticity, wettability, flexibility, and chemical tuneability).

To date, procedures for preparing nanofibres of various materials have included vapour-liquid-solid growth (VLS),[2,12,13] template directed synthesis,[2,14,15] kinetic controlled synthesis,[2,6,16] electrospinning,[17-20] substrate etching, and polymer drawing.[21] While these methods are versatile and provide for proof-of-concept experiments, each has its own limitations. For example, the VLS approach to tailoring fibre dimensionality uses pre-deposited nanoparticle catalyst arrays

that ultimately remain encapsulated in the nanofibre tip potentially altering material properties and hindering future utility. Other limitations such as low yields and the necessity for complex, time consuming lithographic procedures are also significant considerations of these methods.[2]

Surface induced polymerization (SIP) is a versatile technique for controlling surface properties. Materials prepared using SIP have found utility in various applications such as sensors,[22] biomedical devices,[23,24] and chromatographic stationary phases.[25] Moreover, SIP provides materials of controlled polydispersity and high graft density via moderate reaction conditions suitable for preparation of well-defined, functional nanomaterials. Plasma induced polymerization (PIP) is a subset of SIP, where plasma is used to activate a surface that subsequently induces polymerization. Advantages of PIP are its ease of substrate activation, limited material contamination, and rapid processing times. PIP has been employed for synthesis of thin films and coatings,[26-30] but to our knowledge, PIP has not previously been exploited in nanofibre fabrication.

In the present contribution, we demonstrate the straightforward, vapour-phase, PIP of vinyltrichlorosilane to provide well-defined organosiloxane nanofibres of varied dimensionality. The preparation of monolayer and thin films of alkyltrichlorosilane reagents on oxide surfaces is well established;[31-38] however these contributions aim to minimize polymer aggregation via minimal inclusion of moisture and typically employ solution-based procedures. Any comments on polymer aggregation are typically limited to its prevention rather than exploitation

to form 1D materials.[35,37,39] Conversely, we have consciously promoted nanofibre formation by employing standard dry etching as a means to induce vapour-phase surface polymerization while also making no effort to exclude adventitious surface adsorbed water from the reaction chamber. This is the first report for the synthesis of organosiloxane fibres of sub-100 nm diameter that we are aware of.

In preparation for nanofibre growth, n-doped Si (100) wafers (Evergreen Semiconductor Materials) bearing a native oxide surfaces were exposed to oxygen plasma (RIE) in a Plasmalab Microetch RIE 80. This RIE treatment serves a dual purpose; it removes trace organic surface impurities and chemically activates the substrate toward organotrichlorosilane reagents by saturating the surface with hydroxyl moieties. Clean, activated substrates remained in a class 1000 clean room environment of controlled humidity (relative humidity ca. 40%) prior to modification. Vinyltrichlorosilane (VTS), vinyltrimethoxysilane (VTMS), hexyltrichlorosilane (HTS) (Aldrich Chemical Co.), and 5-hexenyltrichlorosilane (Petrach Chemical Co.) were used as received.

For a typical nanofibre synthesis, activated silicon substrates were placed inside a glass desiccator with an adapted vacuum manifold cover. The chamber was repeatedly evacuated and backfilled with Ar (3×) prior to final evacuation to reaction pressure (125 Torr).[40] The Si substrate was covered with a tight sealing, custom designed glass shield and 1.5 mmol of organotrichlorosilane vapour was introduced into the reaction vessel. After 10 minutes the glass shield was raised and the activated substrate was exposed to reagent vapour for 1 hour. Modified

substrates were subsequently removed and stored in ambient conditions. All functionalized wafers were evaluated using scanning electron microscopy (SEM) and energy dispersive X-ray spectroscopy (EDX) using a JOEL 6301F microscope. FT-IR spectroscopy was conducted with a Bruker Vertex 700 Infrared Spectrometer using a "Seagull Variable Angle Accessory", Time of flight secondary ion mass spectrometry (TOF-SIMS) using an Ion ToF IV-100, and X-ray photoelectron spectroscopy (XPS) with a Kratos Axis 165 instrument. Surface aqueous wettability was evaluated with a First Ten Angstroms FTA100 Series contact angle/surface energy analysis system.

SEM micrographs of VTS exposed substrates show well-defined, robust nanofibres of various densities, polydispersities, and lengths (Figure 2-1). Fibre formation and morphology are the result of a delicate interplay between reagent concentration and partial pressure, atmospheric homogeneity, exposure time, and water concentration. As the monolayer functionalization using organotrichlorosilanes,[41] the quantity of surface adsorbed water appears to be the determining factor for promoting nanofibre formation. Control and quantification of this reaction parameter are the subjects of further investigation. Fibres as long as 3 microns have been observed, however typical lengths are approximately 400 - 600 nm (Figure 2-1A). Fibre diameters are uniform across all substrates (ca. 35 nm) and appear to be independent of reaction conditions (Figure 2-1B). EDX confirms the presence of only carbon, silicon and oxygen on the substrate surface.

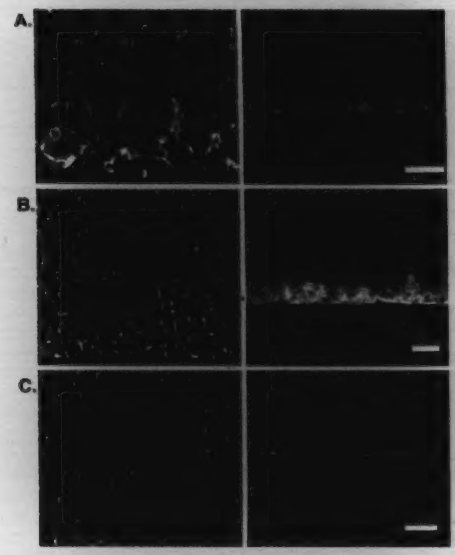

Figure 2-1. Oblique and side view SEM micrographs of a: **A.** high areal density, intertwined network of long fibres showing a ca. 400 nm packed layer. **B.** moderate areal density array of ca. 150 nm long fibres. **C.** low areal density, 100 nm fibres highlighting the uniformity of fibre diameters.

Variable angle FT-IR spectra obtained using an oxygen plasma treated Si(100) wafer background (See Appendix Figure A1- 1) show fibres possess vinyl functionalities (ν_{str} = 3062- 2958, 1602, 1411, and 1279 cm^{-1}, *w*), Si-OH (ν_{str} = 3600 – 3100 cm^{-1}, broad), and Si-O-Si linkages (ν_{str} = 1156-1000 cm^{-1}, *s*); suggesting fibres are crosslinked organosiloxane polymers. Supporting this conclusion, ToF-SIMS analyses present fragmentation patterns with mass-to-charge ratios readily assigned to a variety of vinylsiloxane fragments consistent with a polymer structure (Appendix Figure A1- 2, Figure A1- 3, Table A1- 1). While FT-IR and advancing aqueous contact angle (vide infra) data confirmed

surface functionalization for substrates exposed to VTMS, HTS, and 5-hexenyltrichlorosilane, no fibre structures were observed by SEM (Figure 2-2).

Supporting SEM, EDX, and FT-IR observations, the XP spectra exhibit emissions readily assigned to O(1s), C(1s), Si(1s). The absence of the Cl(2p) clearly indicates full hydrolysis of the Si–Cl bond during the functionalization process and the effective removal of any residual HCl by-products.

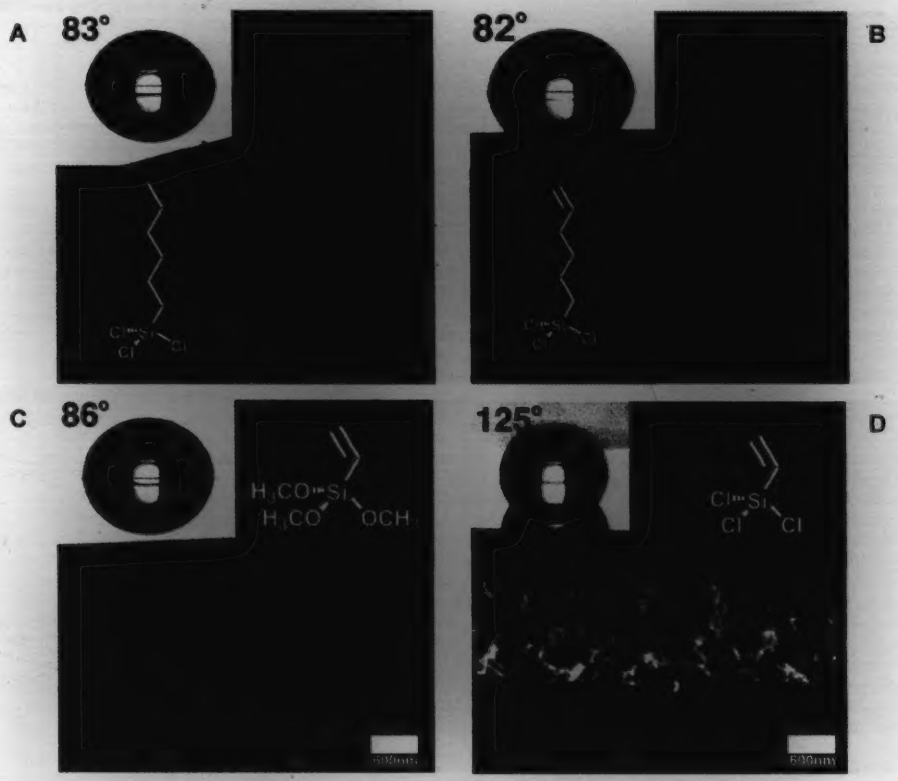

Figure 2-2. The influence of reagent structure on film morphology. Insets. Aqueous advancing contact angle measurements and reagent structures. **A.** HTS, **B.** 5-hexenyltrichlorosilane, **C.** VTMS, **D.** VTS.

Advancing aqueous contact angle measurements provide a direct measure of a substrate surface aqueous wettability (Figure 2-2, insets). Hydrophobicity is a function of liquid drop contact area as described by the modified Cassie and Baxter equation,[42]

$$\cos\theta' = f\cos\theta - (1-f) \qquad (1)$$

where, θ' is the apparent contact angle (CA) on a rough surface, θ is the intrinsic CA on a flat surface, f is the fraction of the solid/water interface, and $(1-f)$ is the fraction of air/water interface. Any increase in the water droplet and solid contact area (*i.e.*, larger f) will increase the aqueous wettability of the rough film surface (*i.e.*, θ' decreases). From this model, it can be readily deduced that introduction of a fibre structure would serve to increase the substrate roughness and decrease f. The ultimate result of this surface modification is that fibre-bearing surfaces would be more hydrophobic than the flat/smooth counterpart (*i.e.*, a surface functionalized with an equivalent chemical functionality). This is exactly what is observed for the present system. (*vide infra*)

Upon treatment with RIE, silicon wafers exhibited an advancing aqueous contact angle (θ') of approximately 0°, consistent with a surface saturated with hydroxyl moieties. After treatment with VTS vapour, fibre-containing substrate surfaces are significantly more hydrophobic (θ'_{VTS} =137°) than smooth VTMS modified substrates (θ'_{VTMS} = 86°) prepared using identical procedures. Clearly, the noted difference in contact angle results solely from the rough fibre structure and highlights the role surface structure plays in a substrate's wetting behaviour.

To further demonstrate the fundamental importance of surface energy and fibre structure on film wetting, a substrate possessing fibres was annealed at 1000° C for 1 hour in air. SEM analysis confirmed this annealing process did not compromise the fibre structure, while XPS showed only trace carbon content indicating removal of any vinyl functionality. The resulting fibre structure was found to be very hydrophilic, $\theta' < 5$. This result is consistent with reports by Bico et al.[43] where the dramatic change in surface wettability arose from both the loss of organic functionality as well as water wetting between the fibres (hemi-wicking). From these observations, it can be concluded that the high contact angle exhibited by the original VTS fibres is the direct consequence of the synergistic influences of high surface area fibre structure and the chemical properties of the surface bonded vinyl moieties. [36,44] Further tailoring of fibre surface chemistry is the subject of ongoing investigation and will provide further insight into these observations.

A reasonable mechanism of fibre formation is summarized in Scheme 2-1. It is well established that OH terminated substrates react with long chain organotrichlorosilanes in solution to form robust, crosslinked, covalently bonded monolayers.[31,36,41,45] Under anhydrous solution conditions, surface adsorbed water on the substrate promotes hydrolysis of organotrichlorosilanes and subsequent crosslinking of the silanol moieties in the plane of the substrate. When activated substrates are exposed to VTS vapour at reduced pressure, Si-Cl bonds respond in an analogous fashion to solution based methods (Scheme 2-1(i)). Steric

considerations limit siloxane surface bonding to a maximum of two surface linkages for each silicon atom.[31,34,46,47] As with solution-based reactions, some crosslinking occurs in the plane of the substrate resulting in monolayer formation. The quality of the siloxane monolayer formed on a substrate depends upon the concentration of surface OH groups on the native oxide. These OH groups limit surface diffusion of physisorbed silanol moieties because of the condensation reaction between the vinylsilanols and OH groups on the surface. Decreased surface diffusion results in small islands of non-equilibrium structures forming on the surface of the substrate.[45] Under these conditions, trace water vapour within the reaction chamber is available to hydrolyze any remaining Si-Cl bonds yielding Si-OH. This Si-OH functionality may further react with VTS to produce organosiloxane chains that assemble to form complex crosslinked fibre structures (Scheme 2-1(ii),(iii)). Fibre growth was not observed for substrates exposed to VTMS, HTS, and 5-hexenyltrichlorosilane. This dependence of surface reactivity on reactant structure is not well understood, however it is reasonable that it may result from the decreased reactivity of organotrimethoxysilane reagents and greater hydrophobicity of longer hydrocarbon chains.

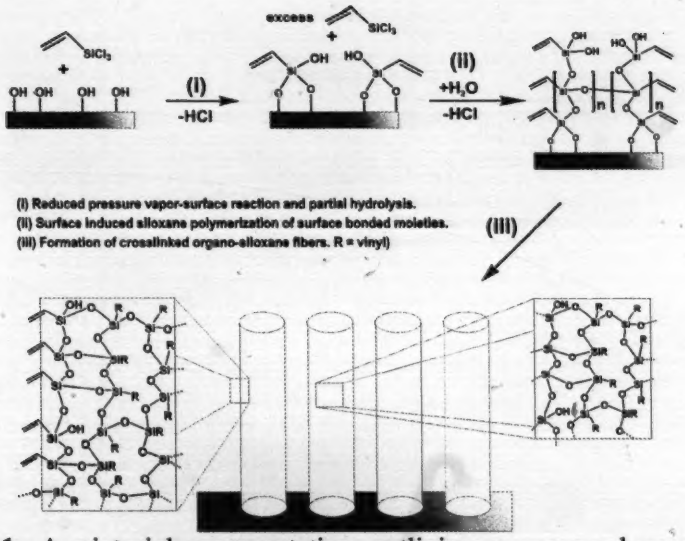

Scheme 2-1. A pictorial representation outlining a proposed mechanism for nanofibre formation.

We have demonstrated that vapour phase PIP affords an effective, straightforward method for introducing 1D nanostructures to substrate surfaces. Spectroscopic analysis highlights that fibres consist of crosslinked organosiloxane polymers that retain chemical functionality which may introduce increased chemical tuneability and access to future applications such as bio-receptors, hydrophobic coatings, and sensors. Additionally, sustained fibre morphology after high temperature exposure may make these materials suitable for refractory applications.

2.2 References

1. Huang, M. H.; Mao, S.; Feick, H.; Yan, H.; Wu, Y.; Kind, H.; Weber, E.; Russo, R.; Yang, P. *Science* **2001**, *292*, 1897-1900.
2. Xia, Y.; Yang, P.; Sun, Y.; Wu, Y.; Kim, F.; Yan, H. *Adv. Mater.* **2003**, *15*, 353-389.

3. Arnold, M. S.; Avouris, P.; Pan, Z. W.; Wang, Z. L. *J. Phys. Chem. B* **2003**, *107*, 659-663.
4. Cui, Y.; Lieber, C. M. *Science* **2001**, *291*, 851-854.
5. Cui, Y.; Wei, Q.; Park, H.; Lieber, C. M. *Science* **2001**, *293*, 1289-1293.
6. Jang, J.; Chang, M.; Yoon, H. *Adv. Mater.* **2005**, *17*, 1616-1620.
7. Virji, S.; Huang, J.; Kaner, R. B.; Weiller, B. H. *Nano Lett.* **2004**, *4*, 491-496.
8. Carter, J. D.; Qu, Y.; Porter, R.; Hoang, L.; Masiel, D. J.; Guo, T. *Chem. Commun.* **2005**, 2274-2276.
9. Zheng, B.; Wu, Y.; Yang, P.; Liu, J. *Adv. Mater.* **2002**, *14*, 122-124.
10. Yu, D. P.; Hang, Q. L.; Ding, Y.; Zhang, H. Z.; Bai, Z. G.; Wang, J. J.; Zou, Y. H.; Zian, W.; Xiong, G. C.; Feng, S. Q. *Appl. Phys. Lett.* **1998**, *73*, 3076-3078.
11. Hu, J. Q.; Jiang, Y.; Meng, X. M.; Lee, C. S.; Lee, S. T. *Chem. Phys. Lett.* **2003**, *367*, 339-343.
12. Verheijen, M. A.; Immink, G.; de Smet, T.; Borgstrom, M. T.; Bakkers, E. P. A. M. *J. Am. Chem. Soc.* **2006**, *128*, 1353-1359.
13. Wang, X.; Ding, Y.; Summers, C. J.; Wang, Z. L. *J. Phys. Chem. B* **2004**, *108*, 8773-8777.
14. Jang, J.; Bae, J.; Park, E. *Adv. Funct. Mat.* **2006**, *16*, 1400-1406.
15. Zhang, M.; Bando, K.; Wada, K.; Kurashima, K. *J. Mater. Sci. Lett.* **1999**, *18*, 1911-1913.
16. Yu, T.; Joo, J.; Park, Y. I.; Hyeon, T. *J. Am. Chem. Soc.* **2006**, *128*, 1786-1787.
17. Li, D.; Xia, Y. *Nano Lett.* **2003**, *3*, 555-560.
18. Deitzel, J. M.; Kleinmeyer, J. D.; Hirvonen, J. K.; Tan, N. C. B. *Polymer* **2001**, *42*, 8163-8170.
19. Doshi, J.; Reneker, D. H. *Journal of Electrostatics* **1995**, *35*, 151-160.
20. Kameoka, J.; Verbridge, S. S.; Jiu, H.; Czaplewski, D. A.; Craighead, H. G. *Nano Lett.* **2004**, *4*, 2105-2108.
21. Jeong, H. E.; Lee, S. H.; Kim, P.; Suh, K. Y. *Nano Lett.* **2006**, *6*, 1508-1513.
22. Abu-Lail, N. I.; Kaholek, M.; LaMattina, B.; Clarck, R. L.; Zauscher, S. *Sensors and Actuators B* **2006**, *114*, 371-378.
23. Kim, J. W.; Chung, C. W.; Rhee, Y. H. *International Journal of Biological Macromolecules* **2005**, *35*, 47-53.
24. Bae, J.-S.; Seo, E.-J.; Kang, I.-K. *Biomaterials* **1999**, *20*, 529-537.
25. Seino, M.; Yokomachi, K.; Hayakawa, T.; Kikuchi, R.; Kakimoto, M.-a.; Horiuchi, S. *Polymer* **2006**, *47*, 1946-1952.
26. Gupta, B.; Hilborn, J. G.; Bisson, I.; Frey, P. *J. Appl. Polym. Sci.* **2001**, *81*, 2993-3001.
27. Gupta, B.; Anjum, N. *Adv. Polym. Sci.* **2003**, *162*, 36-61.
28. Bae, B.; Ha, Y. H.; Kim, D. *Journal of Membrane Science* **2006**, *276*, 51-58.

29. Zhong, S.; Meng, Y.; OU, Q.; Shu, Z. *Plasma Science & Technology* **2006**, *8*, 321-324.
30. Nguyen, V.; Yoshida, W.; Cohen, Y. *J. Appl. Polym. Sci.* **2003**, *87*, 300-310.
31. Sagiv, J. *J. Am. Chem. Soc.* **1980**, *102*, 92-98.
32. Popat, K. C.; Johnson, R. W.; Desai, T. A. *Surface and Coatings Technology* **2002**, *154*, 253-261.
33. Bunker, B. C.; Carpick, R. W.; Assink, R. A.; Thomas, M. L.; Hankins, M. G.; Voigt, J. A.; Sipola, D.; de Boer, M. P.; Gulley, G. L. *Langmuir* **2000**, *16*, 7742-7751.
34. Wasserman, S. R.; Tao, Y.-T.; Whitesides, G. M. *Langmuir* **1989**, *5*, 1074-1087.
35. Yoshida, W.; Castro, R. P.; Jou, J.-D.; Cohen, Y. *Langmuir* **2001**, *17*, 5882-5888.
36. Tsoi, S.; Fok, E.; Sit, J. C.; Veinot, J. G. C. *Langmuir* **2004**, *20*, 10771-10774.
37. Wang, Y.; Ferrari, M. *J. Mat. Sci* **2000**, *35*, 4923-4930.
38. Schwartz, D. K.; Steinberg, S.; Israelachvili, J.; Zasadzinski, J. A. N. *Phys. Rev. Lett.* **1992**, *69*, 3354-3357.
39. Popat, K.; Sharma, S.; Johnson, R. W.; Desai, T. A. *Surf. Interface Anal.* **2003**, *35*, 205-215.
40. No effort was made to free the reaction chamber of surface adsorbed water.
41. Silberzan, P.; Léger, L.; Ausserré, D.; Benattar, J. J. *Langmuir* **1991**, *7*, 1647-1651.
42. Cassie, A. B. D.; Baxter, S. *Trans. Faraday. Soc.* **1944**, *40*, 546-551.
43. Bico, J.; Thiele, U.; Quéré, D. *Colloids and Surfaces A: Physicochem. Eng. Aspects* **2002**, *2006*, 41-46.
44. Tsoi, S.; Fok, E.; Sit, J. C.; Veinot, J. G. C. *Chem. Mater.* **2006**, *18*, 5260-5266.
45. Brunner, H.; Vallant, T.; Mayer, U.; Hoffmann, H. *Langmuir* **1999**, *15*, 1899-1901.
46. Finklea, H. O.; Robinson, L. R.; Blackburn, A.; Richter, B. *Langmuir* **1986**, *2*, 239-244.
47. Senaratne, W.; Andruzzi, L.; Ober, C. K. *Biomacromolecules* **2005**, *6*, 2427-2448.

Chapter 3: Apparatus Development

The original experimental apparatus in which the formation of nanofibers was discovered was very rudimentary. Briefly, oxygen plasma reactively ion etched substrates were placed in a desiccator with a vial of ~ 0.1 mL (0.79 mmol) of VTS. The pressure inside the desiccator was subsequently reduced by application of a vacuum pump for approximately 10 seconds and the wafers were left in the desiccator under reduced pressure and VTS atmosphere for up to 24 hours. The simplicity of the experimental design made it inadequate for further detailed mechanistic investigations as consistent VTS vapour quantity and reaction chamber pressure was not possible with the assembly. Therefore, efforts were directed towards designing an apparatus that isolated and provided control over important experimental parameters that were believed to influence fibre formation.

An early and important observation was the formation of a thick film on the substrate if the VTS boiled violently when the vacuum was applied. We also required an apparatus in which VTS vapour could be introduced to the wafer under static vacuum so that no reagent was being lost to dynamic vacuum. In an effort to address these challenges, we designed and fabricated a Plexiglas® top for the desiccator with four independent access ports. One port was fitted with a Swagelok® valve that connected to a standard Schlenk line double manifold vacuum system. A second port was fitted with hose nipple connector onto which a septum was placed to allow for injection of VTS after a static vacuum of

appropriate pressure was achieved. A vacuum gauge was fixed to the third port to identify the pressure inside the reaction chamber and an aluminum dowel with a Plexiglas® shield connected to the bottom end was placed in the fourth port. With the Plexiglas top placed on the desiccator, the shield could be raised and lowered while the system was under reduced pressure. This modification allowed us to cover the wafer during to injection of VTS to protect it from the being showered with liquid VTS upon injection. It is important to mention that all ports were sealed to make them vacuum tight.

This second apparatus design (App2) provided control of the pressure and VTS quantity inside the reaction chamber as well as the protection of the substrate against the injection of the VTS. With this new apparatus, we were able to determine that lower pressures favoured fibre formation more so than higher pressures; fibre growth was not observed above ~350 Torr. We also noticed that fibres of different spatial density and length were grown on the substrate depending on time the shield covered the substrate after addition of the reagent. This prompted stringent time interval studies on this variable to uncover the reason for this observation. Unfortunately, we were still hampered with irreproducible results; what appeared to be nearly identical reaction conditions quite often produced fibres of very different spatial densities and length or produced thick films on the surface.

While we were conducting reactions with App2 in the spring of 2006 and noticed that we were obtaining polysiloxane films instead of fibres on days when the humidity in the lab was elevated compared to dry winter weather conditions.

These observations lead us to believe that the adsorbed water on the surface of the substrate effected fibre growth in a deleterious manner. To circumvent this, the experimental procedure was modified by heating the wafers in a vacuum oven at 120°C for 2 hours following activation with RIE or piranha. Additionally, the substrates were left in the oven under vacuum until cooled to room temperature. Removal of the surface adsorbed water layer by this method increased the frequency of fibre formation with similar reaction conditions, however, fibres of vastly different lengths and spatial densities were still being produced, especially when the atmospheric humidity changed. We believed that water adsorbed onto the other surfaces in the reaction chamber was also playing a role in the reaction. It was at this point that we decided that water needed to be removed from all surfaces inside the chamber before a reaction was conducted to ensure that the reaction parameters stayed consistent. Unfortunately, the Plexiglas® has a softening temperature of 110°C, and the apparatus top would warp extensively if placed in the oven; warping then prevented the top from forming a tight seal with the desiccator bottom. For this reason, and the others listed below, we needed to modify the design of the chamber.

Because we were designing a new reaction chamber, we needed to consider all the limitations of the Plexiglas® design. The Al dowel used to raise and lower the shield was getting corroded by the HCl vapour produced in the reaction chamber. This corrosion affected the seal formed around the dowel that made the chamber air tight and over time the chamber would rise to atmospheric pressure. Additionally, the Plexiglas® shield had to be at least 2.5 cm thick to withstand the

force of evacuating the chamber while maintaining vacuum. The stress exerted on the plate caused it to gradually deform such that it would not longer fit properly on the desiccator bottom. This thick Plexiglas® plate was extremely costly, and routine remanufacturing was impractical. We also found the injection of VTS through the nipple connector, directly into the vacuum, was cumbersome and resulted in an uncontrolled, rapid injection and vaporization of the reagent. A system designed with an external reagent reservoir was favourable; it would allow for the controlled reagent addition of reagent to the chamber based upon the volatility of the reagent. With all of these factors in mind, the glass sleeve hose connector and glass desiccator top were modified. (Figure 3-1 and Figure 3-2)

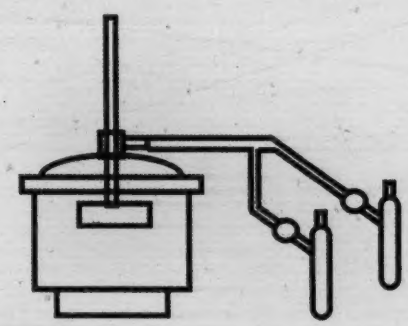

Figure 3-1. Diagram of the apparatus currently being employed for the reaction conducted in Chapter 4.

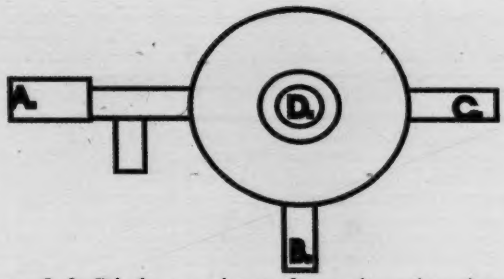

A. Telfon Stopcock
B. and C. Hose Nipple
D. Rod and Gasket

Figure 3-2. Birdseye view of reaction chamber top.

The piece of glass located above the ground glass joint was removed, exposing the inner portion of the ground glass joint. A new sleeve with identical inner diameter to the original was fabricated with a glass manifold added to the top of the sleeve. The manifold was constructed with two hose nipple connectors, a high vacuum Teflon stopcock and a gasket for the shield/dowel piece. A Schlenk flask connected to the manifold top with a minimal length of Tygon® tubing served as the external reservoir for VTS. To replace the aluminium dowel and Plexiglas® shield, a single piece tempered borosilicate glass shield and rod was fabricated. All of the glass pieces readily assemble by feeding the glass rod/shield through the inner diameter of the ground glass joint on the desiccator then through the gasket on the modified sleeve.

Once the glass apparatus (App3) was complete, its internal surfaces were passivated by repeated exposures to VTS vapour. This procedure minimized future reactivity of the reaction chamber and ensured substrates reacting with VTS were exposed to a predictable quantity from reaction to reaction. After the equipment was pre-treated, it was placed in the oven to remove surface adsorbed water prior to every procedure. Reactions conducted with the stringent removal of

surface adsorbed water did not result in fibres on the surface. Clearly, water was a crucial reaction parameter and a controlled quantity of water needed to be added to the reaction chamber if fibre formation was to occur. This required further modification of the apparatus. A second Schlenk flask was added using a glass y-joint branching off the original reagent hose connection. All reactions in Chapter 2 of this thesis were completed with no effort to remove surface adsorbed water. Reactions outlined in Chapter 4 were conducted with App3 with known quantities of water vapour added to the reaction chamber.

Chapter 4: Detailed analysis of the fibre forming process yielding polyvinylsiloxane nanofibres of tuneable dimensions and wettability

The objectives of the work presented in this chapter are outlined here. First, a procedure employing optimized parameters that consistently provided mono-disperse (~35 nm dia.), long (> 500 nm), spatially dense fibres had to be developed. Second, the factors influencing fibre growth needed to be isolated in order to achieve a more comprehensive understanding of the fibre forming process. Third, investigation of organosilane reagents and substrates of varied shapes and compositions was required to expand the versatility of the fibre procedure. Lastly, the wetting properties of the fibre-bearing substrates needed to be extensively investigated.

4.1 Parameter Variation

In order to fully appreciate the findings obtained from experimental parameter variation, a short description of the experimental procedures is included here. Briefly, a previously O_2 plasma reactive ion etched (O_2 RIE) Si wafer with native oxide was placed in the reaction apparatus and the chamber was evacuated to a static base pressure of 125 Torr. Isolated Schlenk flasks connected externally to the reaction chamber were maintained at atmospheric pressure with Ar and loaded with defined quantities of water and VTS. Water was subsequently

introduced into the reaction chamber by vapour transport from the Schlenk flask and allowed to equilibrate for a predetermined time, (t_1). This procedure facilitated the formation of an adsorbed water layer on the substrate surface. Next, a glass shield was lowered over the substrate, the VTS Schlenk flask stopcock opened, and VTS introduced by vapour diffusion into the chamber. After another set period of time, t_2, the shield was raised exposing the substrate to the water/VTS vapour mixture for time, t_3. Scheme 4-1 is a schematic of experimental design including the times, t_1, t_2, and t_3 used in a typical reaction. The volumes of water and VTS that constitute the standard reaction conditions are 50 and 200 μL, respectively. Visual inspection of the substrates following removal from the reaction apparatus provides qualitative information about the fibres formed on the substrate. Substrates bearing fibrous mats that extend less than or equal to 1 μm perpendicular from the substrate are indistinguishable from bare substrates. Substrates with fibrous mats > 1 μm or films > 200 nm in thickness readily diffract light and have a cloudy, white appearance on the surface.

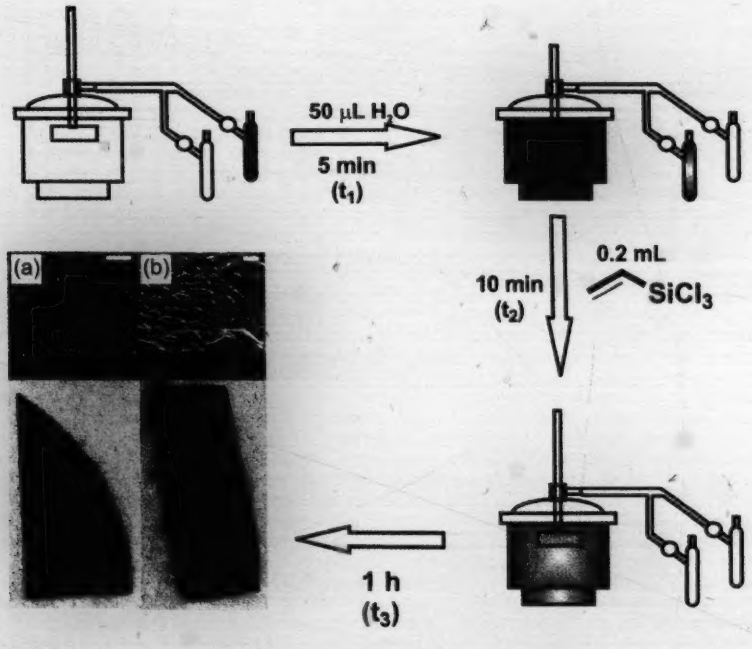

Scheme 4-1. A schematic of the experimental apparatus used for fabrication of polysiloxane nanofibres. Photographs display substrates with (a) a fibrous mat extending ~500 nm off the substrate, and (b) a structured film ~300 nm thick.

Systematic variation of reagent volumes, time intervals, chamber base pressure, as well as the order of reagent addition provided valuable insight into fibre forming process. To expand the scope of this technique, a range of substrates, substrate activation methods, and alkyltrichlorosilanes reagents were also investigated. Length, spatial density and surface topography of the fibre-bearing substrates processed are described as evaluated by SEM.

Substrate Activation

Oxygen plasma reactive ion etching (O_2 RIE) is a procedure commonly used for removing polymeric lithography masks[1] and organic contamination from substrate surfaces.[2] We have previously shown that this technique is also sufficient for activating substrate surfaces in our polysiloxane procedure (See Chapter 2).[3] To extend the versatility of our nanofibre synthetic procedure, we tested other methods commonly employed for substrate cleaning. "Piranha" is a powerful oxidant comprised of a 3:1 mixture of concentrated sulphuric acid and 30 v/v % hydrogen peroxide used extensively in the electronics industry[4] for removing organic contaminates from various substrates. We observed that wafers cleaned in this way yielded fibres of spatial density, length and diameter resembling those obtained using substrates cleaned by O_2 RIE (Figure 4-1a).

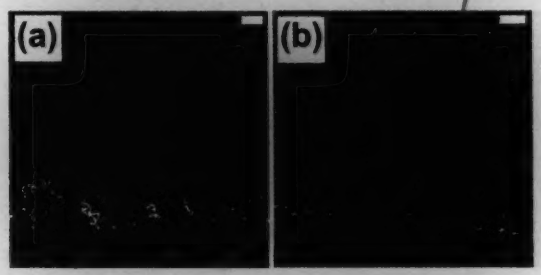

Figure 4-1. SEM images of fibres obtained with (a) piranha cleaning, (b) sonication of substrate in increase polarity solvents: toluene, acetone, isopropyl alcohol, and water. Scale bars are 500 nm.

Substrates were also freed from organic contaminants by sonicating them in a series of solvents with increasing polarity (*i.e.*, toluene, acetone, isopropyl alcohol, de-ionized water) prior to exposing them to water and VTS. SEM images

revealed that these substrates bore fibres, however their spatial density was significantly lower than that observed for substrates activated with RIE or "piranha" solution (See Figure 4-1b).

These observations may be rationalized by considering the efficiency of each cleaning procedure in removing organic contaminants from the substrates and if any surface chemical modification resulted from the individual cleaning procedure. Sufficient removal of adventitious materials from the substrate surface increases the accessibility and subsequent reactivity of surface hydroxyl groups. It is well established that organotrichlorosilanes couple with the hydroxyl functionality and covalently attach to the surface.[5-9] It is reasonable that fibres are coupled to the substrate through surface hydroxyl groups; hence an increased availability of these sites for reaction results in a greater number of fibres being formed. "Piranha" and O_2 RIE treatments are known to be efficient cleaning methods for the removal of organic material from substrate surfaces[2,10,11] and substrates processed with these methods yielded more densely packed fibres. As an aside, it is important to note that substrates must be spin dried following "piranha" cleaning and rinsed with copious amounts of water. Failing to do this leaves sulphate contaminants on the surface[2] that prevent reaction between surface hydroxyl groups and incoming VTS. Visible streaks are observed on the surface of VTS exposed Si wafers (not shown) when substrates are "piranha" cleaned and air-dried. SEM images revealed that the majority of a poorly rinsed substrate was covered with uniform, spatially dense fibres however, at the streak edges, there was very limited fibre growth and a material of ill-defined shape was present that

showed little or no charging; consistent with the presence of surface ionic impurities.

Substrates

After optimizing fibre growth conditions for hydroxyl terminated native oxide Si wafers, substrates of various shape, composition, and surface chemistry were investigated. Native surface oxide passivated Ge(100) and fused quartz were chosen as representative "flat" hydroxylated substrates; commercial silica beads (0.15 μm), fused silica capillary tubes (outer diameter, 358.0 – 359.0 μm), and porous alumina discs (pore diameter, 0.2 μm) were the structured substrates tested.

Surfaces of minimal hydroxyl group concentration were evaluated by passivating Ge(100) and Si(100) wafers with incomplete monolayers of octyltrichlorosilane (OTS). Contact angles measurements of methyl terminated alkyltrichlorosilanes SAMs with varied alkyl chain lengths have been reported by Wasserman *et al.*[6] Well-packed SAMs with alkyl chains greater than three carbons exhibit advancing contact angles of ~ 110°; the OTS SAM functionalized Ge wafers discussed here have advancing and receding contact angles of 93° and 50° respectively. The lower contact angles of these SAM support the conclusion that a non-uniform monolayer was formed. Auger electron spectroscopy (AES) mapping data of the SAM covered substrate confirms a non-uniform coverage of the OTS on the surface as indicated by large regions having high concentrations of Ge concurrent with low concentrations of C. Consistent with this observation, the oxygen concentration is higher in regions where carbon is present because

hydrolysis of octyltrichlorosilane replaces the chlorine moieties with oxygen. Figure 4-2 is a representative SEM and corresponding C, O and Ge AES mapping images of an OTS SAM functionalized Ge wafer.

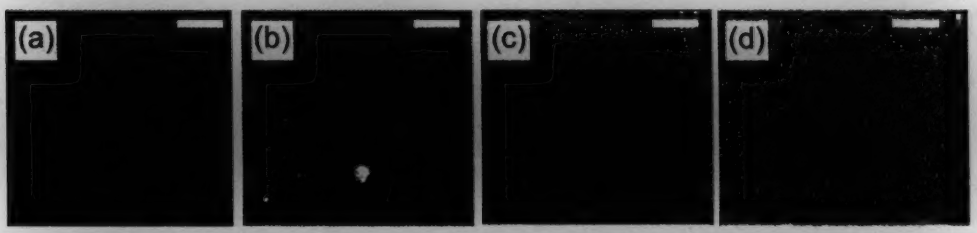

Figure 4-2. SEM (a) and AES mapping ((b) carbon, (c) oxygen, and (d) germanium) of an octyltrichlorosilane (OTS) functionalized oxide passivated Ge(100) wafer. Black regions in the SEM correspond to areas of high carbon and oxygen concentration in the AES analysis. This is consistent with large agglomerates of OTS. AES mapping color scale located to the right of the Ge map; colours at the top of the colour bar correspond to higher intensity of the particular element in that region. Scale bars represent 500 nm.

OTS SAM modified substrates processed using standard polysiloxane fibre growth parameters (*vide supra*) produced fibre structures with variable spatial distribution depending on the quality of the SAM functionalized substrate before exposure to VTS. Substrates coated with more uniform SAMs (not shown) have sporadic fibre growth evenly distributed on their surface with typical diameter (~30 nm) and length (>500 nm). In contrast, wafers incompletely functionalized with OTS have regions both absent of fibres as well as areas of densely packed fibres. Figure 4-3 presents the SEM images obtained after exposing the Ge wafer,

used in Figure 4-2, to VTS. The substrate possesses "holes" where no fibres are present. It is known that SAMs initially form in islands before filling in to generate a complete monolayer.[12] Therefore, a substrate removed from the deposition solution before full functionalization is achieved would be expected to have islands of crosslinked organosilanes present on the surface. The "holes" are observed in the SEM because surface hydroxyl groups are blocked by the surface bonded OTS islands; no fibres are formed in these regions during exposure to VTS. Dense fibres only grow in regions where native oxide surface hydroxyl groups are exposed for reaction with VTS.

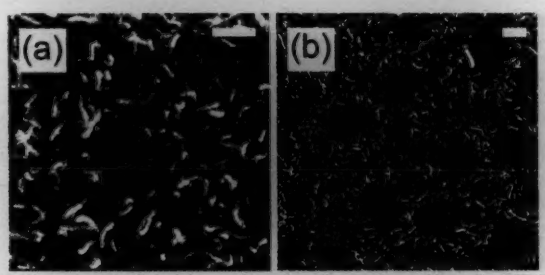

Figure 4-3. SEM images of incompletely functionalized OTS SAM Ge wafers exposed to VTS. It is reasonable that areas where no fibre growth occurs are regions effectively functionalized by OTS. (a) high magnification image showing a single spot where no fibres formed, (b) low magnification image displaying the "holes" absent of fibres. Scale bars are 500 nm.

Fibres were successfully grown on all hydroxyl terminated substrates tested (Figure 4-4). It should be noted that fibres grown on quartz, silica and the capillary tubes typically have larger diameters (~50-70 nm) than those grown on Si wafers (~35 nm). The lengths of fibres fabricated on the capillary tube and quartz are routinely in the range from 5-10 μm in contrast to 1 μm on Si wafers. An

explanation for these dimensional differences is not obvious and is the subject of further study. Nevertheless, these results confirm that hydroxyl group terminated surfaces are required for production of polysiloxane nanofibres in this manner.

Figure 4-4. SEM images of fibres grown on substrates of varied composition and morphology, (a) SiO_2/Si(100) wafer, (b)GeO_2/Ge(100) wafer, (c) porous alumina, (d) high magnification of porous alumina showing fibres inside pores (e) 0.15 μm silica beads, (f) quartz, (g) capillary tube, (h) view of fibres located inside pore of capillary. Scale bars are 500 nm with the exception of images (g) and (h) where they represent 50 and 10 μm, respectively.

In addition to fibre growth on the outer surfaces of the porous alumina and capillary tubes, fibres were also observed inside the pores, growing normal to surface. A survey scan of the entire pore length of porous alumina revealed fibre formation throughout the pore. This demonstrates that our vapour phase fabrication technique provides a convenient method for preparing fibre structures within pores. Many chromatographic and micro-fluidic devices require coatings

placed on the inside of pores. Polysiloxane nanofibres would be well-suited to these applications in light of their high surface area and tailorable surface chemistry. Optimization of this process is the subject of continuing work in our laboratory.

Reagent Quantities

After extensive study, it was found that even small variation in the quantity of VTS reagent dramatically affects fibre growth (Table 4-1). SEM micrographs (Figure 4-5) revealed that when <0.2 mL of VTS was employed, thin films (*i.e.*, thickness ~20 - 100 nm) formed on the substrate. Conversely, using slightly more reagent (ca. 0.25 mL) afforded very small, sparse fibre structures (<100 nm in length), whereas VTS volumes > 0.3 mL result in the formation of rough, thick films (thickness ~50-250 nm).

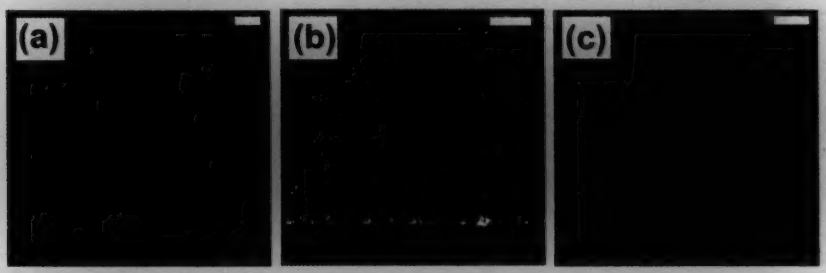

Figure 4-5. Oblique SEM images illustrating the influence of vinyltrichlorosilane volume on fibre formation: (a) 0.15 mL, (b) 0.25 mL, (c) 0.5 mL. Scale bars are 500 nm.

Table 4-1. A summary of the influence water/ silane volumes and time intervals have on the fibre structures produced. Descriptions of the surface structures are assessed by SEM. Reaction conditions affording fibres as described in Entry 1 are adopted as the standard reaction conditions.

Entry	Reaction Parameters					Observations
	Water (μL)	Silane (mL)	t_1 (min)	t_2 (min)	t_3 (min)	
1	50	0.2	5	10	60	near monodisperse (dia. ~30 nm), dense fibres extending ~ 850 nm from substrate surface
2	25	0.2	5	10	60	very thin film with islands < 100 nm in height
3	40	0.2	5	10	60	very thin film (<20 nm) with islands < 50 nm in height, Figure 4-6a
4	60	0.2	5	10	60	thick film (> 250 nm) with smooth rounded contours, Figure 4-6b

5	50	0.1	5	10	60	thin uneven film (20 – 100 nm), rough topography on thick areas
6	50	0.15	5	10	60	thin film (<20 nm) with islands, Figure 4-5a
7	50	0.25	5	10	60	thin film (<50 nm) with short (<100 nm) fibres, Figure 4-5b
8	50	0.5	5	10	60	thick film (>150 nm) with rough features <50 nm in height, Figure 4-5c
9	25	0.1	5	10	60	thin film (<50 nm) with rough features < 50 nm in height
10	100	0.4	5	10	60	thick uneven film (200-500nm) with smooth rounded contours
11	50	0.2	0	10	60	thick film (>150 nm) with smooth features

12	50	0.2	15	10	60	very dense fibres > 500 nm off substrate
13	50	0.2	5	0	60	thick film (>150 nm) with rough topography
14	50	0.2	5	2	60	uneven film (50-150 nm), rough topography with seeding/sparse fibre 100-200 nm off substrate
15	50	0.2	5	5	60	100 nm film with very sparse (1/500 nm^2), long (>1μm) fibres
16	50	0.2	5	8	60	very dense fibres > 700 nm off substrate
17	50	0.2	5	10	5	dense fibres ~ 200 nm of substrate, Figure 4-7a
18	50	0.2	5	10	10	dense fibres ~ 500 nm off substrate, Figure 4-7b
19	50	0.2	5	10	20	dense fibres > 700 nm off substrate, Figure 4-7c

20	50	0.2	5	10	30	dense fibres > 700 nm off substrate

In addition to the aforementioned dependence of fibre growth on the absolute quantity of VTS, we have also determined that even a small adjustment to the water volume gives rise to film formation instead of fibres. When 40 μL of water was used (Figure 4-6), a thin film formed and structures that appear to be nucleating fibres were present. Conversely, when water volumes in excess of 50 μL were used, thick films (>250 nm) with smooth, rounded architectures were obtained. These findings indicate that the amount of water initially present on the substrate surface substantially influences the structural formations that are produced.

Figure 4-6. SEM micrographs showing the thin (<20 nm) and thick (~250 nm) polysiloxane films produced when (a) 40 μL (b) 60 μL of water was used. Scale bars are 0.5 and 5 μm, respectively.

Ratio of Water to Organotrichlorosilane

In an effort to determine if fibre formation results from a specific water:silane molar ratio or instead is imparted by the concentration of reagent in the chamber, the ratio of reagents was halved and doubled (Table 4-1). When decreased by a factor of two, a thin, rough, uneven film (~50 nm) is obtained. When the reagent quantities were doubled, a thick film (200 – 500 nm) with smooth rounded features was produced. To understand these observations, it is important to consider what is happening at the surface of the wafer; when altering the water content in the chamber, the thickness of the adsorbed water layer changes because the volume to chamber surface area ratio has been modified. Therefore, it can be concluded that the thickness of the adsorbed water layer plays a crucial role in the production of fibrous structures.

Order of Reagent Addition

To further support the concept that an adsorbed water layer was required for fibre formation, the order of reagent addition to the reaction chamber was reversed. No fibres formed on the substrate when VTS was admitted to the chamber before the water (not shown). This confirms the necessity of the surface adsorbed water layer for fabrication of organosilicon nanofibres by this method.

Chamber Pressure

To initiate and promote fibre growth, the pressure in the reaction chamber must be low enough to facilitate full evaporation of VTS. If the base pressure exceeded 350 Torr, at 21°C, the VTS did not fully evaporate. Consequently, there was not enough reagent present for fibre formation to occur, and only a thin film

(<20 nm) was observed. This is consistent with our observations regarding the influence of organotrichlorosilane volatility on fibre formation (*vide infra*).

Influence of t_1 ,t_2, t_3

It has also been determined that the time intervals between introduction of reagents, t_1 and t_2, and the substrate exposure time, t_3, affect the fibre production. To reiterate, t_1 denotes the time that water was allowed to equilibrate in the reaction chamber prior to introduction of VTS. The second time interval, t_2, was the duration that the shield covered the substrate after VTS entered the desiccator, and t_3 was the substrate exposure time. (See Scheme 4-1)

When t_1 = 0 min, a thick film (>250 nm) with smooth rounded contours was obtained and no fibres were formed. If t_1 > 5 min, dense fibre growth was observed. It is evident from this that water equilibration time is a major factor in fibre production. Since water vapour entered the room temperature apparatus, the majority of the water initially physisorbed to the chamber surfaces. While equilibrating, a portion of the water re-entered the vapour phase; our results imply the adsorbed water layer is thicker at t_1 = 0 then at t_1 = 5 min. Hence, fibres do not form if the water layer is too thick. (*vide infra*)

Likewise, VTS vapour must disperse within the reaction chamber if fibre growth is to be realized. If t_2 = 0 min, a thick (>150 nm) uneven film was obtained and no fibre growth was observed. Extending t_2 to 5 min yielded a small number of fibres scattered across the surface; spatially dense fibres were not obtained until t_2 = 8 min. If VTS vapour was allowed to stand for extended periods (*i.e.*, t_2 >15 min), uneven films with rough areas and nucleation sites were

seen. (Table 4-1) To rationalize these findings, one must appreciate that there is a rapid, large change in reagent concentration when the VTS vapour initially enters the reaction vessel. This and our apparatus design causes a high concentration of VTS near the substrate surface before it diffuses throughout the chamber. Because fibres do not evolve until t_2>8 min, we conclude that growth is most significant when the delivery of VTS to the substrate surface is diffusion limited.

While somewhat expected, it has also been determined that fibre length relies on the time the substrate is exposed to VTS. If t_3 = 5 min, 200 nm fibres were produced, longer fibres (~ 500 nm) were obtained after 10 min, and finally micron long fibres resulted with t_3 > 20 min. There was no appreciable difference in spatial density of the fibres with extended reaction time (t_3) upon visual inspection of the SEMs. Figure 4-7 shows SEM images illustrating the dependence of fibre length on t_3.

Figure 4-7. Cross-sectional SEM images demonstrating the increased length (ℓ) of fibres with longer exposure times to VTS: (a) t_3 = 5 min, ℓ ~ 200 nm, (b) t_3 = 10 min, ℓ ~500 nm, (c) t_3 > 20 min, ℓ ~ 1.1 μm. Scale bars are 500 nm.

Variation of Organotrichlorosilane Reagents

In Chapter 2 it was noted that fibre growth was not observed with 5-hexenyltrichlorosilane (5HTS), hexyltrichlorosilane (HTS), and vinyltrimethoxysilane (VTMS). These results can be attributed to either the low vapour pressure or low reactivity of the reagents. Considering reagents are introduced to the chamber by evaporation and subsequent vapour diffusion, reagent volatility is the determining factor for efficient delivery of the reagent to the substrate. That is, a reagent's volatility is what ultimately governs the concentration of reagent in the chamber. A volatile liquid has a high vapour pressure and consequently low boiling point. Comparing the boiling points of the above reagents (5VTS 198 °C; HTS, 191 °C; VTMS, 123 °C) to VTS (92 °C), it is clear all are significantly less volatile. Therefore, these reagents will diffuse into the reaction chamber at a slower rate than VTS, leading to a lower concentration in the vapour phase. With this in mind, we deduce 5-hexenyltrichlorosilane and hexyltrichlorosilane are not volatile enough to support fibre growth at room temperature. Consistent with our conclusions that volatile $RSiCl_3$ reagents are required for fibre synthesis , Seeger *et al.* produced nanofibres on Si wafers using vapour phase methyltrichlorosilane (b.p. 64°C).[13] While VTMS has a more comparable boiling point to VTS, the slower hydrolysis of trimethoxysilanes[8] makes it unsuitable for nanofibre formation with the present conditions. Recently, we have obtained structures that appear to be the nucleation seeds of fibres (SEM, Figure A1- 5) when using butyltrichlorosilane (BTS, b.p. 142°C) as well as very

sparse, short fibres (ℓ < 100 nm) when using 3,3,3-trifluoropropyltrichlorosilane, (FTS, b.p. 114°C). These features resemble those previously observed when reaction parameters were not optimized for VTS; hence, a logical extension of this work is to determine the most favourable reaction conditions for promotion of BTS and FTS fibres.

Copolymerization

The small fibres observed when FTS was employed as a precursor initiated our exploration into co-polymerization of VTS and FTS. Our work thus far has focused on gradient block co-polymer formation; this was achieved by the sequential addition of FTS to the chamber once a VTS reaction was initiated. With this protocol, extremely long, very dense fibres were produced (SEM, Figure 4-8). XPS analysis of the substrate confirms the presence of Si, O, C, and F. In addition, the absence of the Cl peak indicates that all Si-Cl bonds were hydrolysed. High resolution XPS of the carbon region shows two peaks; the higher energy component corresponds to carbon bonded to fluorine atoms.

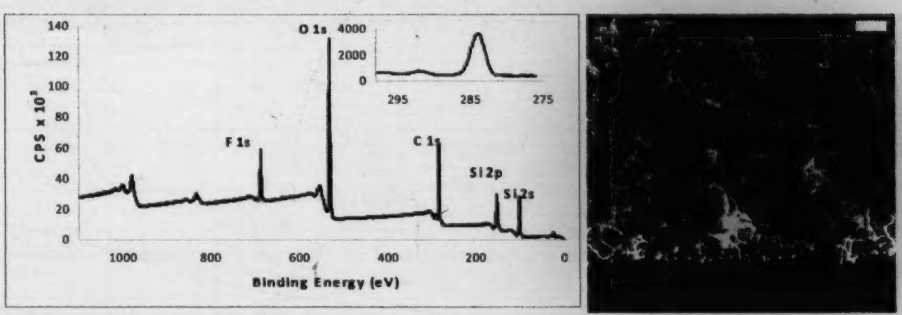

Figure 4-8. A survey XP spectrum of VTS/FTS co-polymer fibres displaying the peaks corresponding to Si, C, O, and F. Inset, high-resolution spectrum of the

carbon 1s region. The higher energy peak observed in the C 1s high-resolution spectrum is due to fluorine atoms bonded to the third carbon of the propyl group on 3,3,3-trifluoropropylsilane. SEM of the co-polymer fibres. Scale bar is 500 nm.

Completely random polymerization of VTS and FTS requires the volatility of each reagent to be roughly equivalent so that their respective concentrations in the chamber are approximately equal. In order for this adjustment to be made, the equipment, and or procedure must be altered to apply either a constant even heating or reduced pressure to the FTS. Investigations in this area are the subject of further work in our laboratory.

4.2 Mechanism of Formation

Based upon the observations outlined in this chapter, we propose the following fibre growth mechanism. It is important to note that reaction conditions very similar those used herein are often employed for vapour phase formation of siloxane bonded SAMs.[14,15] For this reason, much is learned about the formation of nanofibres by comparing our procedures and findings to those of researchers studying SAM formations.

It is reasonable that incoming VTS molecules are completely hydrolyzed either in the vapour phase or adsorbed on the substrate surface. Subsequently, hydrolyzed VTS (h-VTS) molecules are physisorbed to the surface water layer by hydrogen bond interactions. Due to the inherent instability of this state,[9] the silanol moiety of the h-VTS reacts with a surface hydroxyl group via a condensation reaction, anchoring the h-VTS to the surface. However, the three

hydroxyl groups on the h-VTS cannot simultaneously couple to the surface because the density of hydroxyl groups on a native oxide silicon surface is not high enough to accommodate three silanol condensations on one molecule.[6] This leaves one, or possibly two, silanol groups of h-VTS available for coupling with other physisorbed h-VTS moieties. At this point the steric constraints imposed on the alkyl chains of each VTS by the crosslinking reaction between two h-VTSs must be considered. It has been reported that the maximum bond length of a Si-O-Si bond is 3.2 Å if the bond angle is 180°, while the van der Waals diameter for C is 3.5 Å.[16] Therefore, when two h-VTS molecules crosslink, the alkyl chains must arrange to minimize the interaction between the otherwise overlapping van der Waals radii of the alkyl chains.[8,17,18] By assuming this configuration, the remaining hydroxyl group is positioned away from the substrate, and is in a suitable orientation to direct further condensation reactions normal to the substrate. Subsequent coupling of these newly surface bonded h-VTS molecules with additional h-VTS leads to the formation of polymeric islands on the surface of the substrate. Essentially, the initial anchoring of h-VTS creates a nucleation site for island formation.[19] The newly formed polymeric network protrudes from the substrate surface, so that incoming VTS molecules come in contact with the islands more readily than with the water layer. This vertical polymerization produces complex crosslinked fibre structures. If the incoming VTS molecules do not react with the polymeric networks growing away from the surface, they will reach the water layer on the surface, physisorb and eventually condense with other h-VTS moieties to form a film between the islands. Hence, the critical factor for

fibre formation must be the rapid nucleation and growth of the polymeric islands vertical to the surface. An illustration of the fibre forming process is provided in Scheme 4-2.

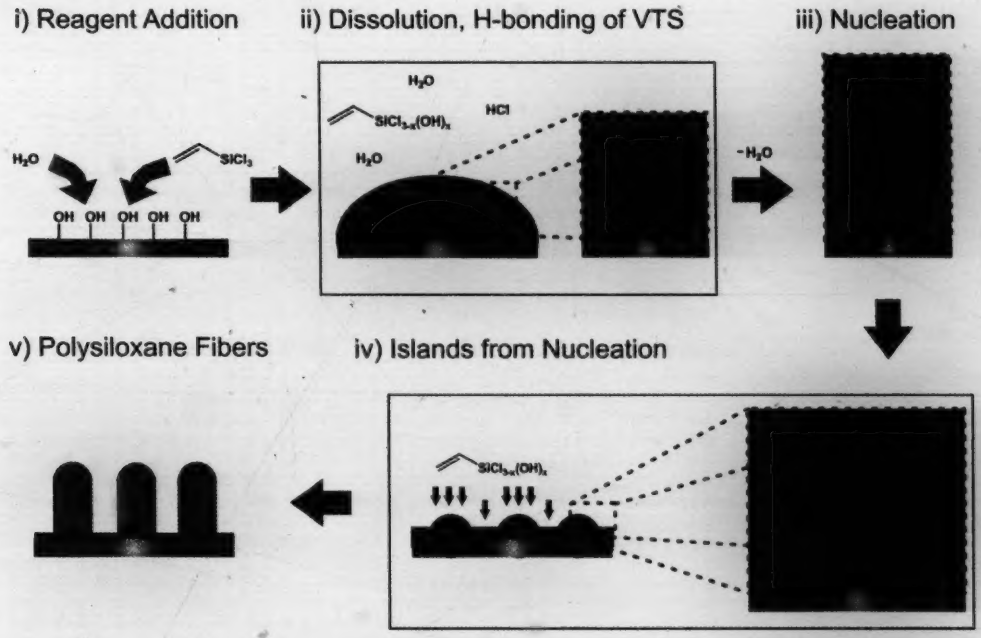

Scheme 4-2. An illustration depicting the fibre forming process: i) addition of H_2O, VTS; water adsorbs to the surface of the substrate, ii) some h-VTS dissolves in water adsorbed layer, hydrogen bonds with surface hydroxyl groups, iii) H-bonded h-VTS couples with surface hydroxyl groups, eliminates H_2O, then other dissolved h-VTS moieties crosslink with surface bound h-VTS, iv) polymeric islands emerge as further crosslinking with incoming VTS occurs, v) vapour phase VTS preferentially couples to the islands that have emerged from the adsorbed water layer due to their greater surface area and accessibility, otherwise VTS dissolves in water layer and crosslinks with other VTS moieties forming a thin film.

From this proposed mechanism it can be seen that the concentration of surface hydroxyl groups dictates the spatial density of the fibres grown because they are nucleation sites for vertical polymerization. The concentration of hydroxyl groups on the native oxide surface of a Si wafer is 5 OH/nm^2.[6] Based upon our observations of fibre-bearing Si/SiO_2 wafers, we conclude that this concentration is adequate to support the formation of dense, mono-disperse fibres. Fibre density is reduced when a surface with fewer accessible hydroxyl groups is employed. The reaction performed on a Ge wafer with an incomplete OTS SAM illustrates this point effectively; surface bound OTS reduces the concentration of surface hydroxyl groups resulting in a decreased spatial density of fibres (Figure 4-3). In absence of conclusive evidence, it is also reasonable that there is an upper limit to the concentration of hydroxyl groups for fibre formation. If there is a surface hydroxyl density greater than the packing density of VTS molecules the result would be increased bonding. This would lead to minimal singly bonded VTS functionalities thereby limiting crosslinking between h-VTS moieties and fibre growth. Additionally, if polymeric islands that form during the early stages of film growth are in close enough proximity they may couple together resulting in film formation in lieu of fibres.

Following our rational stepwise variation of all the known and controllable reaction parameters, we propose that a major factor governing the nucleation of polymeric islands is the concentration of h-VTS in the surface adsorbed water layer. As stated above, when silanol groups anchor to the surface in the appropriate geometry, nucleation points are created from which non-equilibrium

islands form. Incoming VTS and/or h-VTS bond onto the top of these islands and polysiloxane networks are formed that grow away from the substrate surface. Since h-VTS must anchor to the surface if polymeric islands are to form, the concentration of h-VTS molecules interacting with the surface adsorbed water determines if rapid nucleation and growth occurs.

The effect of water and reagent quantities, as well as t_1, and t_2 can be understood in the context of the concentration of h-VTS in the adsorbed water layer; we have established that fibre growth does not occur if the concentration is outside a narrow range. Recall, that if $t_1 < 5$ min, no fibre growth was observed. Under these conditions, the water has not established equilibrium in the reaction chamber, thus a large quantity of water is adsorbed onto the substrate surface leading to a low concentration of VTS (h-VTS) at the surface. A similar situation arises if more than 50 μL of water is used; a thick water layer forms. Under these conditions, the number of h-VTS molecules anchoring to the surface, as well as those available to crosslink and promote fibre growth is decreased. As a result, the rate of island formation is reduced such that, vapour phase VTS molecules react evenly across the surface adsorbed water layer.

Consistent with our observations, the influence of adsorbed water on surfaces on solution functionalization of vinyltrimethoxysilane (VTMS) has been investigated by Cohen *et al.*[20] In this report they determined that organosilane surface coverage decreased when the surface adsorbed water layer had a thickness greater than 2 monolayers. For larger amounts of adsorbed water, it was proposed

that penetration of the VTMS through the water layer to the substrate hydroxyl groups became increasingly difficult due to the hydrophobicity of the vinyl group. As a result, VTMS molecules condensed in the thick water layer without attachment to the surface hydroxyl groups forming a film. It is interesting to note that Cohen and co-workers also observed polymeric island structures forming on the substrates with dimension of approximately 22 nm diameter and 10-20 nm in height when under certain conditions. The lack of fibres extending from the surface is mostly likely due to a larger energy penalty associated with the increased polymer-liquid interfacial area with respect to the polymer-vapour interface formed in our system.

When the VTS quantity is in a large excess (*i.e.,* 0.50 mL) or the VTS is not uniformly dispersed in the reaction chamber ($t_2 < 8$ min) the surface adsorbed water layer becomes saturated in h-VTS and rough, uneven films are produced. In this case, a large number of h-VTS molecules anchor to the surface, producing islands that are so closely spaced that crosslinking between islands occurs concomitantly with vertical polymerization. Polymerization in both directions impedes fibre growth.

Our findings (Table 4-1) suggest that the optimal concentration of VTS near the surface is diffusion limited ($t_2 > 8$ min). As a result of equipment design, when the stopcock for the VTS flask is opened to the chamber, a high local concentration of reagent exists near the substrate. This affect is further accentuated by rapid VTS evaporation under reduced pressure. A shield covering the substrate prevents the VTS from hydrolyzing in the adsorbed water layer

before the concentration close the surface of the substrate has diminished to the appropriate value for fibre formation.

The islands observed when using BTS can be rationalized appropriately with this mechanism as well. The formation of islands on the surface suggests that the concentration of BTS in the surface adsorbed water layer is within the appropriate range for promoting vertical fibres, however there is not enough BTS to propagate the growth vertical to the surface. One possible explanation for this is the rate of fibre formation is slower and the investigated exposure time (1h) may be too short for the BTS reaction. Given that the butyl chain is longer than the vinyl group (C_4 vs. C_2), it is more hydrophobic. This structural difference will alter its solubility in and diffusion through the surface adsorbed water layer. Consequently, the anchoring of BTS to the surface via terminal hydroxyl groups is impeded. In this respect, it is reasonable that longer exposure times may be required for the fabrication of BTS fibres.

In summary, the key points governing the production of fibres: thickness of the adsorbed water layer, local concentration of VTS at the substrate surface, and finally the dissolution and surface attachment of VTS to direct polymerization normal to the surface.

Patterning

We have exploited our mechanistic knowledge of the fibre forming process by confining the fibre growth to specific regions on the substrate. This was accomplished by patterning the surface of a Si wafer with FTS using a polydimethylsiloxane (PDMS) stamp. Fibre growth was severely reduced in the

regions stamped by the PDMS (Figure 4-9). Further efforts in the fabrication of hierarchical roughness and physical property investigations of these structures are ongoing in our lab.

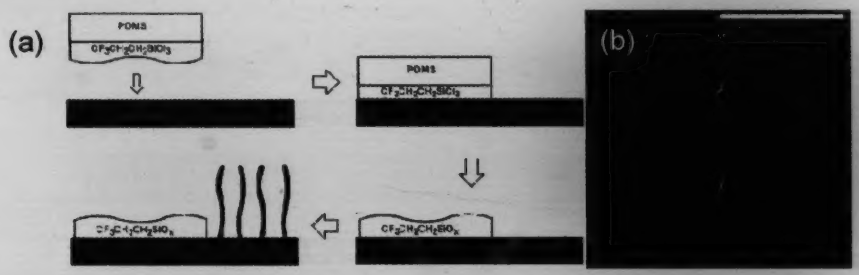

Figure 4-9. (a) Cartoon depicting the PDMS stamping process used to pattern the Si wafer. Left side of Si substrate stamped with 3,3,3-fluoropropyltrichlorosilane (FTS) before exposure to VTS. (b) SEM image showing a successfully patterned region of the Si wafer. Nanofibres preferentially grow an areas of the substrate not stamped with FTS. Scale bar is 50 μm.

Functionalization:

To further increase the hydrophobicity of our surfaces, a fibre-bearing substrate was solution functionalized with FTS. We found however, that as-prepared fibres crosslink upon exposure to organic solutions, with the assistance of FTS. The reduced surface roughness associated with the crosslinked fibres resulted in a smaller advancing contact angle than for the as-prepared fibres. In an effort to prevent fibres from crosslinking, a calcination step was introduced. Calcination serves two functions: it increases the rigidity of the fibres by converting them to SiO_2 as confirmed by XPS, and it surface terminates the newly formed oxide fibres with hydroxyl groups. The oxide fibres were subsequently functionalized via a

solution-based procedure with FTS. The XP spectrum of the FTS functionalized fibres exhibits a peak with binding energy characteristic of F 1s (687.10 eV) (Figure 4-10) and a C 1s peak with two components (284.5, 291.7 eV) on account of the carbon bonded to the fluorine atoms and adventitious carbon. The carbon bonded to F atoms is expected to have a higher binding energy because of the strong electron withdrawing capabilities of the fluorine atoms. SEM of the modified fibres (Figure 4-10) shows that the fibre morphology has been maintained after solution functionalization and no obvious film growth was observed.

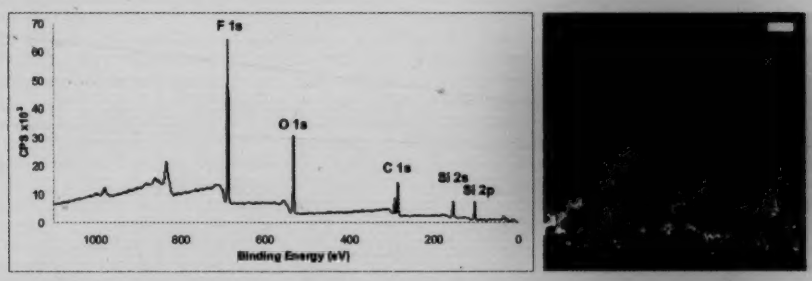

Figure 4-10. X-ray photoelectron spectrum (left) and SEM image (right) of nanofibres calcined at 500°C that were subsequently solution functionalized with 3,3,3-fluoropropyltrichlorosilane. Scale bar is 500 nm.

Functionalized fibres were also characterized by ToF-SIMS and compared to that of the as prepared fibres (Appendix Figure A1- 6). Fragments with m/e⁻ ratios corresponding to silica as well as the alkylfluorosilanol are present in the spectrum.

4.3 Tailored Wettability

In Chapter 2, the significance of surface roughness induced by the fibrous structure on wettability by directly contrasting the advancing contact angles for a substrate bearing fibres and a smooth substrate functionalized with the same material was clearly highlighted. An important point warranting further discussion in this area is the influence of fibre spatial density and length on roughness and subsequent wettability.

Recall, as a droplet of liquid makes contact with a surface, three interfaces with corresponding free energies, γ_{SV} ,γ_{SL}, and γ_{LV}, are formed, where SV, SL, and LV, respectively, are the solid-vapour, solid-liquid and liquid-vapour interfaces. Young's equation[21] is the simplest expression for rationalizing the wetting of a surface by a liquid droplet. θ is defined as the contact angle formed when a droplet of water comes to rest on a substrate.

$$\cos\theta = \frac{\gamma_{SV} - \gamma_{SL}}{\gamma_{LV}} \qquad (1)$$

For a hydrophilic surface, $\theta < 90$,

$$\frac{\gamma_{SV} - \gamma_{SL}}{\gamma_{LV}} > 0 \qquad (2)$$

and the energy of the solid-liquid interface is less than the energy of the solid-vapour interface. Alternatively, when

$$\frac{\gamma_{SV} - \gamma_{SL}}{\gamma_{LV}} < 0 \qquad (3)$$

$\theta > 90$, and $\gamma_{SV} < \gamma_{SL}$, the surface is deemed hydrophobic. However, Young's model is only applicable for flat, chemically homogeneous substrates.

To account for the effects of surface roughness, and/or chemical heterogeneity on wettability, two different adaptations have been proposed. Wenzel's adaptation[21] compensates for the increased surface area arising from roughness at the solid-liquid interface by introducing a roughness factor, *r*, representing the actual surface over geometric surface area.

$$\cos\theta_{rough} = r\cos\theta_{smooth} \qquad (4)$$

Wenzel proposed that the increased surface area associated with rough topography resulted in a greater intensity of the interface energy at the surface, *i.e.*, γ_{SL} is larger for a rough surface than the chemically analogous smooth surface. In the case where the surface has a strong affinity to water, roughness under the drop will further decrease the net energy associated with spreading, and the drop will wet the surface more readily. For the opposite situation, there exists a net increase in energy for wetting the surface by the drop of water, so this will be unfavourable.

The second adaptation, the Cassie-Baxter model,[22,23] considers a substrate with a chemically heterogeneous surface. This accommodates two possible situations, the first being a flat, chemical heterogeneous surface, and the second being when surface roughness is so great that a droplet of water sits on top of the asperities instead of conforming to them as predicted by Wenzel's theory.

$$\cos\theta = f_1\cos\theta_1 + f_2\cos\theta_2 \qquad (5)$$

where f_1, f_2 are the area fractions of each component (*e.g.*, air and solid) with $f_1 + f_2 = 1$. From this equation, it can be seen that a smaller fraction of water in contact with the solid will lead to greater hydrophobicity.

For the present system, substrate roughness is a direct consequence of the fibre spatial density and length. Substrates with low spatial density and short fibres will have a smaller surface area than those bearing long fibres of high spatial density. The question that arises, which model, Wenzel or Cassie, provides a more accurate description of the wettability of the surface? It is been suggested that moderately hydrophobic surfaces, θ slightly above 90°, behave in a Wenzel-type fashion[24] since air-liquid interfaces are not favoured in this region, however some reports of Cassie-type behaviour are in the literature.[15]

To definitively classify the substrates bearing fibres prepared in the present study to either of these models, it is necessary to obtain direct roughness measurements of the surface. Unfortunately, the flexibility and intertwined structure of polysiloxane fibres precludes accurate determination of these values. In this regard, an alternative method must be considered. Quéré *et al.*[24] have extensively contrasted the two models by studying the hysteresis of the advancing, θ_a, and receding, θ_r, contact angles. Low θ_r result when the drop pins to the surface roughness[24] which ultimately increases the adhesion of the drop to the surface. In this light, a larger contact area between the droplet of water and the surface of a material will greatly increase its adhesion. A droplet conforming to surface roughness (Wenzel) will have a lower θ_r and consequently, larger

hysteresis than one that rests on top of the roughness (Cassie).[25] How a droplet of water behaves on a surface is then characterized by the contact angle hysteresis, $\Delta\theta$. Static contact angle measurements taken for substrates having fibres of various densities and lengths are shown in Figure 4-11. It is readily seen that fibres of decreased spatial density and length have lower θ_a and θ_r than those of long, dense fibres. Substrates possessing the short, moderately dense fibres (Figure 4-11a) have a higher surface area than substrates having sparsely distributed fibres (Figure 4-11b) and as such will have a larger contact area with the drop. For this reason, the θ_r is lower for the short, moderately distributed fibres.

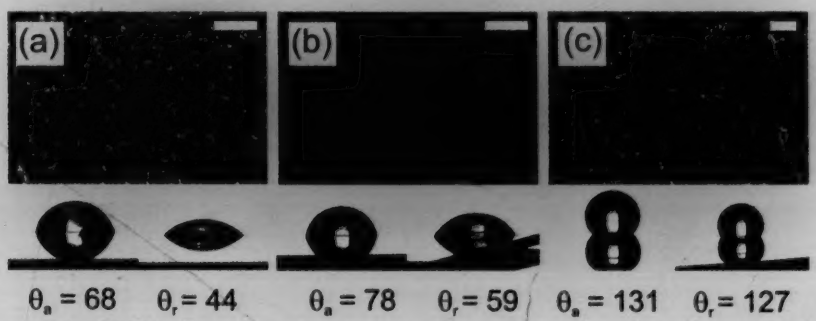

Figure 4-11. SEM images and corresponding contact angles demonstrating the effect of fibre length and spatial dispersion on wettability of the substrate: (a) moderately dispersed fibres ~200 nm in height, (b) sparsely distributed fibres ~100 nm in height, (c) densely packed fibres ~1 μm in height. Scale bars are 500 nm.

The θ_r of the short, sparse fibres (Figure 4-11b) is much lower than the θ_r of the long, dense fibres (Figure 4-11c) and as such the contact area must be larger for the short fibres. Since the smaller fibres have less surface area associated with them, the drop must be conforming to the roughness to have a larger contact angle. That is, the short, sparsely distributed fibres are not adequate for supporting an air-

liquid interface. Long, densely packed fibres display $\theta_r = 127 \pm 2°$, which suggests a Cassie wetting mechanism. Recall, a high θ_r is indicative of a lower contact area; for this condition to be met, the drop must be resting on top of the surface structure. Our observations of Cassie type wetting are not surprising as other densely packed, long fibres have been reported to respond in the same manner.[13] From the above findings, it is clear that spatial density and fibre length determine the effective roughness of the substrate which subsequently governs the wetting regime of the substrate. Substrates bearing short, dense fibres have lower contact angles than short sparse fibres, which are less hydrophobic than long, densely packed fibrous substrates.

Surface water repellency was increased when the fibrous structure was combined with the low surface energy associated of fluorinated surfaces. Both the FTS functionalized oxide fibres and the co-polymer fibres of VTS/FTS exhibited superhydrophobicity ($\theta_a = 161°$, 152°, respectively). Receding angles are not reported because of inherent difficulties associated with obtaining accurate θ_r for extremely hydrophobic surfaces with the goniometer employed for the present measurements. Based on the qualitative observation that water bounces off a surface bearing copolymer fibres (Figure 4-12), we conclude that this surface exhibits a larger θ_r than the solution functionalized oxide fibres. It is reasonable that the lower receding angle observed for the functionalized oxide fibres arises from incomplete functionalization with FTS.

Figure 4-12. A stream of water rebounding off the surface of a Si wafer bearing co-polymer fibres of VTS/FTS. The reflection of the stream and water droplets is observed on the wafer.

An important point to stress is both Wenzel and Cassie-Baxter models relate interfacial contact area to the substrate wetting behaviour. Another approach receiving increased attention of late expresses the contact angle in terms of the contact line, that is, the location of the three-phase equilibrium, instead of interfacial contact area. Various reports have been published [23,26-32] rationalizing wettability in terms of the contact line. This is in response to the inability of both Wenzel and Cassie models in predicting experimental contact angles of certain topographies. In the interest of providing a comprehensive discussion, the wetting behaviour of the substrates is also explained using the contact line.

The description of wetting in the context of the contact line has many corollaries to the Wenzel and Cassie models; both roughness and surface heterogeneity at the contact line influence the predicted behaviour of a water droplet on a substrate. As surface roughness increases, it reaches a critical value, changing the equilibrium at the contact line, thereby increasing the contact angle.[28] For hydrophobic surfaces, γ_{SL} is larger than γ_{SV}; accordingly, a smaller linear

fraction of asperities on the contact line increases the contact angle. Moreover, a decreased linear fraction of asperities destabilizes the contact line. This instability lowers the energy barrier to displacing the drop, therefore the drop can travel more freely on the surface.[26,31] For a truly hydrophobic surface, both the advancing and receding angles need to be large.

Extrand developed a series of equations based on contact line interactions to predict the advancing and receding contact angles of liquids both suspended and collapsed onto surfaces with regular geometry.[33] In doing so, he also defined the critical contact line density of regular asperities above which a drop will be suspended and below, will collapse into the surface features. These equations were derived by balancing the body and surface forces when a drop is placed on a rough surface. The critical line density was found to be proportional to the apparent and true contact angles as well as the surface, density, and volume of the liquid drop. The slope of the asperity relates the true contact angle to the apparent contact angle. These equations were used calculate the contact angles for substrates with asperities of different length, spacing, slope, and geometry and compared to measured values. His equations more closely predicted the advancing and receding contact angles and hysteresis than either the Wenzel or Cassie models. An important finding of this study was that rise or slope of the asperities as well as their width and spacing are the most significant factors affecting the wetting behaviour.

For drops suspended on surface roughness, the θ_a increases with a larger rise angle of the asperities, and the θ_r increases as the linear fraction of asperities

on the contact line decreases. With collapsed drops, increased roughness results in larger θ_a than smooth surfaces of similar chemical composition and the increased linear fraction leads to lower θ_r. In both cases, the hysteresis is increased with the asperity contact and the severity of the edge angles (asperity rise).

Although Extrand's equations cannot be directly applied to our systems due to the irregularity of the nanofibres on substrates, parallels can be drawn between the systems regarding the changes in contact line and consequent contact angle imposed by the geometry of rough features. We deduce that the short, sparsely distributed fibres seen in Figure 4-11 are unable to suspend the drop of water. As a result, the drop conforms to the rough features and the contact line is the interface between the solid and the liquid. The continuity of the contact line increases its stability and the receding angle decreases. Because fibres are sparse on the surface, the roughness compared to more spatially dense fibres is decreased hence, a smaller advancing contact angle is observed. Conversely, long, densely packed fibres exhibit high θ_a and θ_r, behaviour characteristic of drops suspended on top of asperities. Because the water drop is resting on a mat of randomly oriented fibres, an erratic topography exists at the contact line which increases the advancing contact angle. With the drop suspended, the asperities have a smaller linear fraction on the contact line than the collapsed drops. The concomitant decreased contact line stability is marked by the higher receding angles. Our findings are in accordance with the high advancing and receding contact angles previously obtained for dense, randomly distributed fibrous topographies.[30,34,35]

We have demonstrated that the wetting behaviour of the polysiloxane nanofibres can be successful rationalized using both the contact line and area models. We believe that both methods are acceptable due to the even distribution of fibres on the surface of the substrate. In instances where this criterion is not satisfied, the contact line method may be invoked.

Hydrophobic Stability of Fibres

Wettability of fibre-bearing substrates transforms from ~ 130° to <5° after storage in normal atmospheric conditions (T~20 °C, RH ~ 40%) for approximately three months. This observation is opposite to what is expected as atmospheric organic contaminants adsorbed onto the surface over time often increase the hydrophobicity and contact angle of the substrate. To rationalize this behaviour one must consider that the polysiloxane fibres are of composed of a siloxane backbone with a vinyl substituent as well as some remaining hydroxyl moieties; both hydroxyl and vinyl functionalities are potentially present on the substrate surface. Over time, atmospheric moisture is adsorbed into the fibre structure. In doing so, water coats the fibre surface where hydroxyl moieties are present making it more hydrophilic. As a result, when a contact angle is measured, the water droplet is drawn into the fibrous mat instead of resting on top of the asperities. In addition, water is also capable of hydrolyzing the surface siloxane bonds to form surface silanol functionalities,[36] which further increases the hydrophilic nature of the fibres and decreases the angle observed for a droplet of water on the surface. Supporting the adsorption proposal, heating the substrates under vacuum at 120°C for at least one hour drives off surface adsorbed water and the substrate becomes

hydrophobic once again. It should be noted that the contact angle does not return to its initial value. Two explanations exist that explain this observation: 1. Surface silanols require temperatures > 120 °C to transform back to surface siloxane bonds[37], so the surface has a greater concentration of surface hydroxyls than when is was initially prepared, and 2. the vinyl side chains are slowly being oxidized by UV light to produce diol moieties. Both these options introduce more hydrophilic functionalities onto the surface of the fibre.

Conclusions:

The critical parameters which promote fibre production have been isolated and a detailed mechanism for fibre formation has been presented. It is clear from the present study that water equilibrium and slow addition of VTS are vital if fibres are to be formed. We have also established that substrates must possess hydroxyl terminated surfaces for fibres to grow. Fibres nucleate when hydrolyzed VTS moieties couple with surface hydroxyl groups to form polymeric islands. These islands emerge from the adsorbed water layer as more hydrolyzed VTS react with the polymeric islands. Additional VTS molecules diffusing to the substrate surface preferentially couple to the islands due to the large surface area resulting in fibre growth normal to the surface. As hydroxyl groups must be accessible to react with VTS and subsequently grow fibres, substrates must be cleaned to remove organic contamination. Both oxygen plasma and piranha are suitable for activating oxide terminated substrates, as both adequately remove organic contamination and increase the effective concentration of surface hydroxyl groups. The aqueous wetting behaviour of the substrate was also shown to be a

function of the spatial density and length of the fibres. Finally, co-polymers of VTS/FTS were fabricated and patterning capabilities were demonstrated.

4.4 Experimental Procedures

Concentrated sulphuric acid (98%) and hydrogen peroxide, 30 v/v % were obtained from Fisher Scientific and used without further purification. Toluene purification was achieved using a Innovative Technologies PureSolv® solvent purification system with alumina columns. Vinyltrichlorosilane (VTS), butyltrichlorosilane (BTS), 3,3,3-trifluoropropyltrichlorosilane (FTS) and octyltrichlorosilane (OTS) were used as received from Aldrich Chemical Co. Si (100) test wafers (n-doped (P), 1-100 Ω·cm) were obtained from Evergreen Semiconductor Materials. Optical grade fused quartz wafers purchased from Esco products and alumina membrane discs (0.2μm) acquired from Whatman. Un-doped Ge (100) wafers (10 - 45 Ω·cm) were purchased from MTI Corp. Bangs Labs was the supplier of 0.15μm silica beads suspended in water and polyimide coated fused silica capillary tubes with an inner diameter range of 72.0 – 74.0 μm and outer diameter of 358.0 – 359.0 μm were purchased from Polymicro Technologies. The PDMS mask was obtained as a gift from the University of Alberta Nanofab.

Substrate Preparation and Activation

Substrates were activated by the removal of organic contaminants with one of three methods: oxygen plasma reactive ion etch (RIE), oxidative piranha solution, or sonication in solvents of increasing polarity. For RIE, the plasma

chamber was first purged for 30 min with 80% of 100 sccm of O_2 and 75% of 300 W radio frequency at 150 mTorr. The substrate was then treated with the O_2 plasma under similar conditions for 90 sec. Piranha cleaned wafers were submerged in the 3:1 H_2SO_4:H_2O_2 solution for 30 min then rinsed with de-ionized water and spun-dry at 4000 rpm for 30 sec. Care should be taken when handling this solution as it is highly corrosive and reacts violently with organics. Wafers cleaned by sonication in solvents of increasing polarity (toluene, acetone, isopropyl alcohol, de-ionized water) were sonicated for 3 minutes each. Ge wafers and porous alumina discs were activated using RIE. Following activation, substrates were placed in a vacuum oven (125 Torr, >120°C) for a minimum of two hours prior to modification and remained under vacuum until reaction.

Commercially available silica beads (Bangs Labs) were supported on Si wafers to facilitate their reaction with VTS under reduced pressure. Mono and multi-layers of silica beads were prepared by spin coating 0.1mL of 0.15μm beads suspended in water at 4000 rpm for 30 seconds onto a previously piranha cleaned Si wafer. The substrate was placed in the vacuum oven (125 Torr, >120°C) for >2 hours to facilitate crosslinking of the beads to the native oxide surface. Finally, the bead coated substrates were activated by treatment with RIE and surface adsorbed water was removed by heating in the vacuum oven for 2 hours.

The polyimide coating was removed from the silica capillary tubes by submerging capillaries in boiling concentrated sulphuric acid for >10 min. The capillaries were subsequently rinsed 3 times with de-ionized water then left to soak

in de-ionized water for 10 min before flame drying. Since the capillaries were stored in a regular laboratory setting, capillaries were additionally piranha cleaned before being used to remove any contamination adsorbed from the atmosphere. After piranha and rinsing with copious amounts of water, the capillaries were also placed in the vacuum oven to dry before reaction with VTS.

OTS SAMs were fabricated by placing vacuum oven dried Ge wafers, previously RIE cleaned into a 1.5mM solution of OTS in dry toluene under inert atmosphere. Wafers remained in the silane solution for 2 hours before being rinsed thoroughly with toluene and dried in the vacuum oven at 120°C for 1 hour.

Patterned substrates were fabricated by stamping a piranha cleaned wafer with 3,3,3-trifluoropropyltrichlorosilane coated on a polydimethylsiloxane (PDMS mould). The patterned wafer was then placed in the vacuum oven at 120°C for >1hour to remove any surface adsorbed water.

Polysiloxane Nanofibre Synthesis

The reaction apparatus was placed in a 150°C for at least 2 hours before being used for a reaction. When equipment was removed from the oven, it was immediately assembled and placed under vacuum while cooling to prevent any water adsorption. Once cooled to room temperature, the desiccator was backfilled to atmospheric pressure with Ar and cooled, activated silicon substrates were placed inside the glass desiccator with adapted manifold top (Scheme 2-1). The equipment was evacuated again, and while under dynamic vacuum, flame dried to remove any water adsorbed during the assembly stages, before finally leaving the

chamber at a static base pressure of 125 Torr. Two Schlenk flasks connected externally to the reaction chamber were backfilled to atmospheric pressure before being charged separately with 2.7 mmol de-ionized water (50 μL) and 1.5 mmol of organotrichlorosilane (200 μL). Next, the de-ionized water flask was opened to the reaction chamber, and water introduced to the chamber by evaporation using direct flame. After a predetermined amount of time (t_1), the Si substrate was covered with a tight sealing, custom designed glass shield and the organotrichlorosilane vapour was introduced to the reaction vessel by opening the stopcock to the silane reagent Schlenk flask. After a second induction time, (t_2), which allowed the silane reagent adequate time to evaporate, the glass shield was raised, exposing the activated substrate to reagent vapour (t_3). Standard reaction times were t_1 = 5 min, t_2 = 10 min, t_3 = 60 min. Modified substrates were subsequently removed and stored in ambient conditions.

VTS/FTS co-polymer synthesis

Gradient co-polymer nanofibres of VTS/FTS were prepared using similar conditions with the following modifications. Once the Si substrate had been exposed to VTS for 10 min the VTS Schlenk flask stopcock was closed and the flask was backfilled with Ar. Next, 0.92 mmol (150 μL) of FTS was injected into the flask and the protective glass shield in the reaction chamber was lowered to cover the Si substrate. The stopcock was re-opened and 5 minutes elapsed before the shield was raised to expose the Si wafer to the organotrichlorosilane vapour for 24 hours.

Solution Functionalization with FTS

FTS functionalized nanofibres were fabricated by solution phase functionalization of calcined fibres with FTS. Nanofibres were calcined to remove any organic functionality and to decrease the flexibility of the fibres. Calcination was accomplished by heating fibre bearing substrates at 500°C for 1 hour with a heating rate of 25°C/min. Following calcination, the fibre bearing substrate was placed in an unstirred 20 mM solution of FTS in dry toluene for 24 hours kept under Ar.

Secondary Electron Microscopy

Secondary Electron Microscopy images were obtained by first sputter coating a ~1 nm film of Cr onto the substrates using an Edwards Xenosput XE200. Microscope images were obtained using a JOEL 6301F field emission secondary electron microscope with an accelerating voltage of 5kV.

Contact Angle Measurements

Advancing and receding contact angle measurements were obtained using a First Ten Angstroms FTA100 Series contact angle/surface energy analysis system using de-ionized water as the probe liquid. The average of three measurements taken at different locations on the substrate ensured representative values were recorded.

X-ray Photoelectron Spectroscopy

A Kratos Axis Ultra instrument operating in energy spectrum mode at 210W was used for XPS measurements. The base pressure and operating chamber pressure were maintained at $\leq 1 \times 10^{-7}$ Pa. A monochromatic Al Kα source was used to irradiate the samples, and the spectra were obtained with an electron

takeoff angle of 90°. Wide survey spectra were collected using an elliptical spot with 2 mm and 1 mm major and minor axis lengths, respectively, and 160 eV pass energy with a step of 0.33 eV. Sample compositions were determined from the peaks of the survey spectra with subtracted linear background using the internal instrument values of relative sensitivity factor. Sample charging was minimized using an electron gun.

Time of Flight – Static Secondary Ion Mass Spectroscopy

Time of Flight – Static Secondary Ion Mass Spectrometry was conducted on an Ion ToF IV-100.

Auger Electron Spectroscopy

The Auger measurements and SEM images associated with AES were carried out using JAMP-9500F Auger microprobe (JEOL). The instrument is equipped with Shottky field emitter, which can obtain 3 nm and 7.5 nm spatial resolutions for SEM and Auger mapping, respectively. The accelerating voltage and emission current for both, the SEM and Auger imaging were 25 kV and10 nA, respectively. The working distance was 23 mm. The sample was rotated 30 degrees away from the primary electron beam to face the electron energy analyzer. The Auger peaks of Ge LMM (1143 eV), C KLL (263 eV), and O KLL (503 eV) were selected for Auger imaging. The intensity of each pixel in the Auger image was calculated by (P – B)/B, where P and B are the peak and background intensity, respectively. Such intensity definition helps to reduce the edge effect of islands and dots. An auto probe tracking technique was used to compensate for possible drifting of the image during the analysis as a result of power instabilities.

4.5 References

1. Williams, K. R.; Gupta, K.; Wasilik, M. *J. Microelectromech. Syst.* **2003**, *12*, 761-778.
2. Kern, W. *J. Electrochem. Soc.* **1990**, *137*, 1887-1892.
3. Rollings, D. E.; Tsoi, S.; Sit, J. C.; Veinot, J. G. C. *Langmuir* **2007**, *23*, 5275-5278.
4. Kern, W. *Handbook of Semiconductor Wafer Cleaning Technology - Science, Technology, and Applications*; William Andrew Publishing/Noyes: New Jersey, 1993.
5. Sagiv, J. *J. Am. Chem. Soc.* **1980**, *102*, 92-98.
6. Wasserman, S. R.; Tao, Y. T.; Whitesides, G. M. *Langmuir* **1989**, *5*, 1074-1087.
7. Carson, G.; Granick, S. *J. Appl. Polym. Sci.* **1989**, *37*, 2767-2772.
8. Kessel, C. R.; Granick, S. *Langmuir* **1991**, *7*, 532-538.
9. Silberzan, P.; Leger, L.; Ausserre, D.; Benattar, J. J. *Langmuir* **1991**, *7*, 1647-1651.
10. Mun, S. Y.; Jang, Y. S.; Ko, Y. S.; Huh, S. B.; Lee, J. K.; Jeong, Y. H. *J. Electrochem. Soc.* **2006**, *153*, G866-G869.
11. Sirghi, L.; Kylian, O.; Gilliland, D.; Ceccone, G.; Rossi, F. *J. Phys. Chem. B* **2006**, *110*, 25975-25981.
12. Onclin, S.; Ravoo, B. J.; Reinhoudt, D. N. *Angew. Chem. Int. Ed.* **2005**, *44*, 6282-6304.
13. Artus, G. R. J.; Jung, S.; Zimmermann, J.; Gautschi, H. P.; Marquardt, K.; Seeger, S. *Adv. Mater.* **2006**, *18*, 2758-2762.
14. Hoffmann, P. W.; Stelzle, M.; Rabolt, J. F. *Langmuir* **1997**, *13*, 1877-1880.
15. Dong, J.; Wang, A.; Ng, K. Y. S.; Mao, G. *Thin Solid Films* **2006**, *515*, 2116-2122.
16. Jorgensen, W. L.; Maxwell, D. S.; Tirado-Rives, J. *J. Am. Chem. Soc.* **1996**, *118*, 11225-11236.
17. Stevens, M. J. *Langmuir* **1999**, *15*, 2773-2778.
18. Rye, R. R.; Nelson, G. C.; Dugger, M. T. *Langmuir* **1997**, *13*, 2965-2972.
19. Rye, R. R. *Langmuir* **1997**, *13*, 2588-2590.
20. Yoshida, W.; Castro, R. P.; Jou, J.-D.; Cohen, Y. *Langmuir* **2001**, *17*, 5882-5888.
21. Wenzel, R., N. *Ind. Eng. Chem.* **1936**, *28*, 988-994.
22. Cassie, A. B. D.; Baxter, S. *Trans. Faraday. Soc.* **1944**, *40*, 546-551.
23. Gao, L.; McCarthy, T. J. *Langmuir* **2007**, *23*, 3762-3765.
24. Lafuna, A.; Quéré, D. *Nature Materials* **2003**, *2*, 457-460.
25. Martines, E.; Seunarine, K.; Morgan, H.; Gadegaard, N.; Wilkinson, C. D. W.; Riehle, M. O. *Nano Letters* **2005**, *5*, 2097-2103.
26. Öner, D.; McCarthy, T. J. *Langmuir* **2000**, *16*, 7777-7782.
27. Extrand, C. W. *Langmuir* **2003**, *19*, 3793-3796.
28. Bartell, F. E.; Shepard, J. W. *J. Phys. Chem.* **1953**, *57*, 455.

29. Swain, P. S.; Lipowsky, R. *Langmuir* **1998**, *14*, 6772-6780.
30. Gao, L.; McCarthy, T. J. *Langmuir* **2006**, *2006*, 2966-2967.
31. Chen, W.; Fadeev, A. Y.; Zhsieh, M. C.; Öner, D.; Youngblood, J.; McCarthy, T. J. *Langmuir* **1999**, *15*, 3395-3399.
32. Mansky, P.; Lui, Y.; Huang, E.; Russell, T. P.; Hawker, C. *Science* **1997**, *275*, 1458-1460.
33. Extrand, C. W. *Langmuir* **2002**, *18*, 7991-7999.
34. Gao, L.; McCarthy, T. J. *J. Am. Chem. Soc.* **2006**, *128*, 9052-9053.
35. Zhu, L.; Xiu, Y.; Xu, J.; Tamirisa, P. A.; Hess, D. W.; Wong, C.-P. *Langmuir* **2005**, *21*, 11208-11212.
36. Bausch, G. G.; Stasser, J. L.; Tonge, J. S.; Owen, M. J. *Plasmas Polym.* **1998**, *3*, 23-34.
37. Sneh, O.; George, S. M. *J. Phys. Chem.* **1995**, *99*, 4639-4647.

Chapter 5: Future Directions – Potential Functional Materials

The body of work presented in Chapters 2 and 3 of this thesis involved the characterization and investigation into the fibre forming process of polysiloxane nanofibres formed via surface induced polymerization of vapour phase reagents. With a reasonable knowledge of the growth process in hand, the future direction of this project includes the investigation of these nanofibres as functional materials. In the following sections, examples of some practical chemical and structural modifications of polysiloxane fibre structures that can be envisioned are provided. These modifications may be classified into three categories: functionalization of the as-prepared materials, modification of the Si precursor to provide functional materials, and assembly of hierarchical structured materials. A logical starting point is to access the as-prepared fibres for their potential modification.

5.1 Functionalization of currently prepared materials

5.1.1 Vinyl Group Functionalization

As mentioned earlier, the vinyl pendant group offers further derivatization using well established olefin reactions. The benefit of employing coupling reactions post-polymerization is the physical properties intrinsic to the material are not altered by the functionalization but the reactivity of the surface can be manipulated. A scheme illustrating select examples of reactions that are accessible with the olefin functionality are presented in Figure 5-1.

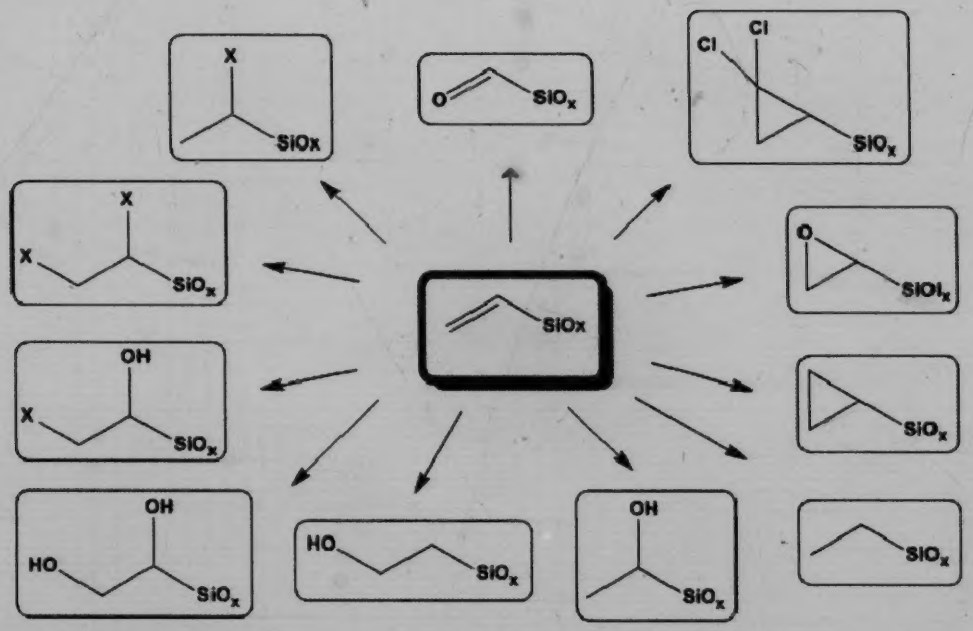

Figure 5-1. Traditional organic reaction pathways accessible with olefin groups. Details of the reactions can be found elsewhere. [112]

Halides and hydroxyl groups can be introduced via straightforward electrophilic addition reactions. Aldehyde, carboxylic acid, or epoxide functionalities are accessible using oxidation reactions. From here, nucleophilic substitution and addition reactions could be employed to graft functional molecules (*vide infra)* to the polysiloxane fibres via carbon-carbon bonds. Alternatively, ether, ester, and amide coupling reactions are also possible (Figure 5-2, Figure 5-3).

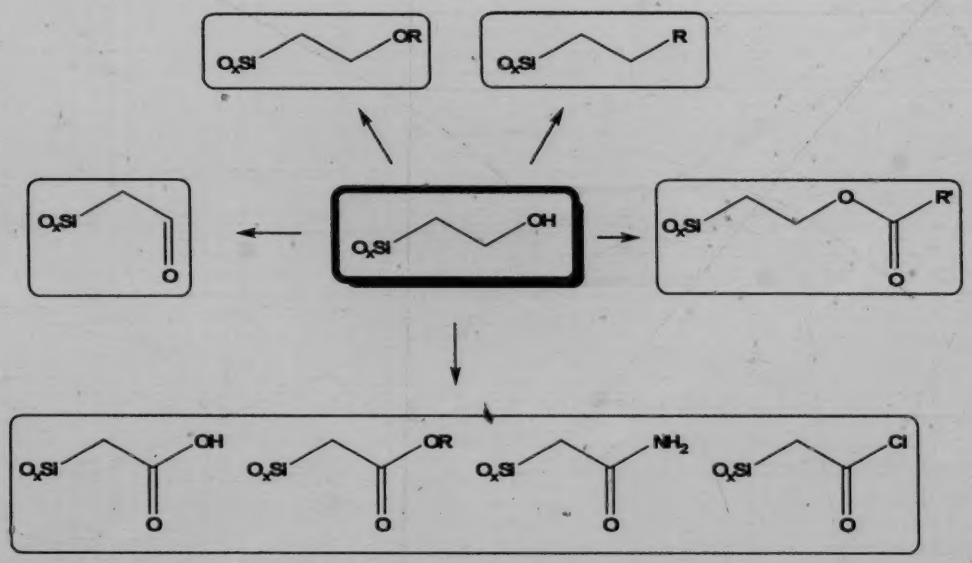

Figure 5-2. Representative organic transformation available for 1° alcohol obtained through the electrophilic addition to an olefin .[112]

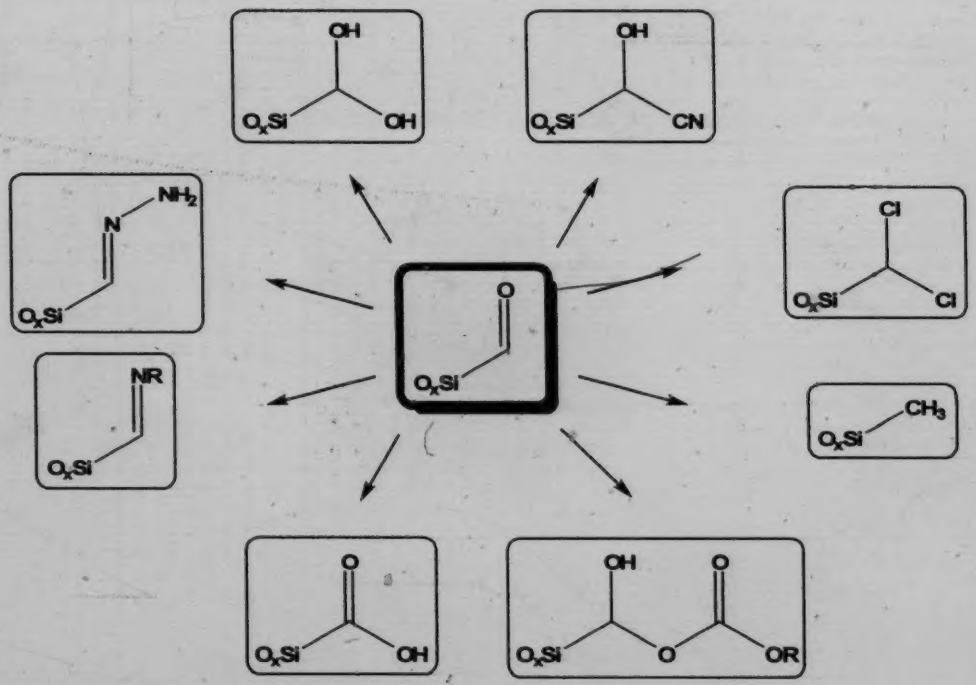

Figure 5-3. Various reaction pathways available with an aldehyde.[112]

The presented list of reactions is in no way meant to be comprehensive, but instead illustrates the versatility afforded by the vinyl and hydroxyl groups.

5.1.2 Functional Materials Accessible By Coupling to Surface Functionalities of the Polysiloxane Nanofibres

The reaction pathways presented above demonstrate the numerous options available for coupling molecules to the surface of polysiloxane fibres and subsequently altering the surface chemistry of the fibres. Recently, the potential of functionalizing polysiloxanes has been realized with the fabrication of a chiral stationary phase by coupling chiral moieties to a polysiloxane matrix.[113] It is not unreasonable then, to propose functionalizing polysiloxane nanofibres for this and

other purposes. Additionally, polysiloxanes could be fabricated on medical implants with bioactive molecules to promote successful incorporation of the implant into the body.

Because polysiloxane nanofibres have high aspect ratios and high surface areas, it is also reasonable that they could function well as catalytic supports. Additionally, calcined fibres can be functionalized via the surface hydroxyl group for ultimate use as high temperature catalytic supports. High surface area, mesoporous silica has been shown to be an effective support for a Ru complex used as a transfer hydrogenation catalyst.[114]

5.1.3 Poly(vinylsiloxane) as a precursor to Silicon Carbide

SiC is an interesting material because of its wide bandgap (2.39 – 3.33 eV), high temperature stability, thermal conductivity, saturated drift velocity, and resistance to breakdown in an electric field. [115] Adding to these favourable properties SiC is also chemically and mechanically robust. These properties make SiC an ideal active material for use in high temperature, high power, and high frequency devices such as field-effect gas sensors, MOSFETs, transistors, and Schottky diodes.[115] In addition, SiC emits in the visible blue region of the electromagnetic spectrum and was used in the first commercial blue LED.[115] There has been an increased interest in SiC nanofibres as electron emitters for field emission displays.[116]

The mechanical stability of SiC has made it a common reinforcement agent in ceramic/composite materials.[117] Studies have shown that the strength of SiC

increases with decreasing size and has been attributed to a decrease in the number of crystal defects associated with smaller dimensions.[118]

All of the above characteristics make 1D SiC a fascinating material to investigate. Still, to facilitate more comprehensive fundamental studies and before device applications are to be fully realized, various methods for the synthesis of controlled dimension 1D nanofibres must be developed. The traditional method for fabricating SiC is the carbothermal reduction of SiO_2, called the Acheson Process. This procedure uses resistive heating of a graphite rod placed in a trough of silica and coke. The mechanism of the process[119] is shown in Scheme 5-1:

$$C(s) + SiO_2(s) \longrightarrow SiO(g) + CO(g)$$
$$SiO_2(s) + CO(g) \longrightarrow SiO(g) + CO_2(g)$$
$$C(s) + CO_2(g) \longrightarrow 2CO(g)$$
$$2C(s) + SiO(g) \longrightarrow SiC(s) + CO(g)$$

Scheme 5-1. Mechanism for the formation of silicon carbide by carbothermal reduction of silica with coke using the Acheson process.

This strategy has been applied to 1D SiC fabrication and employ nanoscale precursors or templates such as carbon nanotubes/particles[120-123] or mesoporous silica.[124] Other methods commonly employed include chemical vapour deposition,[125,126] combustion synthesis,[127] vapour-liquid-solid growth,[128] and arc-discharge.[129] Another method uses single source precursors with pre-existing silicon carbon bonds. More specifically polysilanes, polycarbosilanes and polyorganosiloxane have all been employed.[130-132] Cai *et al.*[133] pyrolyzed polydimethylsiloxane under a flowing stream of Ar at low temperatures (1050 °C)

to provide crystalline SiC core, amorphous SiO_2 shell nanofibres. More specifically and more related to the polysiloxane nanofibres outlined herein, microfibres of melt-spun pinacolborane modified polyvinylsiloxane fibres were pyrolyzed to give SiC microfibres.[134] Single source precursors offer the advantage of providing high ceramic yields while delivering single-phase, crystalline SiC. This stems from the fact that polymers can be designed with the appropriate ratio of Si:C.[131] It is reasonable then that the present polyvinylsiloxane nanofibres may be viable precursor materials for 1D SiC. Moreover, the intrinsic formation of nanofibres by our method eliminates the electro-spinning or melt-spinning step typically used with polymeric precursors.

The only further requirement of the present system is the substrate on which the fibres are fabricated must withstand the temperatures required for formation of crystalline SiC. Based upon literature reports, typical processing temperatures exceed >1100 °C.[132,135,136] More recently, we have successfully fabricated fibres on porous alumina disks (mp 2054 °C). Porous alumina discs have the additional advantage of being readily dissolved in both acidic and basic media. This property offers the potential to isolate the ceramic fibres for use in composite materials.

5.2 Modification of Si Precursor

5.2.1 · $R_{4-x}SiCl_x$

The structure of a siloxane polymer is dictated by the pendant organic functionality on the monomer. Nomenclature for monomer functionality used here is as follows: monofunctional, R_3SiX, difunctional, R_2SiX_2, trifunctional, $RSiX_3$, and quadrifunctional, SiX_4 where X represents a site capable of coupling with another monomer.[3] Polymers fabricated with difunctional monomers produce linear chains, tri- and quadrifunctional monomers form three-dimensional crosslinked networks, and monofunctional monomers end-cap chains in both cases. As the extent of branching and crosslinking increases, the structure of the polysiloxane transforms from linear chains to three dimensional polymeric networks. With increased crosslinking, the rigidity of the polymer increases and the flexibility decreases. Polysiloxane nanofibres fabricated in this work consist of three dimensional siloxane networks arising from the tri-functional reagent, VTS (See Chapter 2). It is reasonable that the flexibility of the polysiloxane fibres can be tailored by the addition of organochlorosilane reagents of varied functionality (*i.e.*, R_2SiCl_2, $SiCl_4$) to the reaction chamber during fabrication of the VTS fibres. Tuneable flexibility would be very advantageous for example in the design of dry adhesives (*vide infra*).

5.2.2 Variation of R, Si

Silicon rich oxides (SRO), composite materials of nanocrystalline Si (nc-Si) /SiO_2, are attractive materials to study due to their size-dependent optical and electronic properties.[137]

Previous work in the Veinot group[137] has shown that hydrogen silsequioxane (HSQ), a molecules with silicon to oxygen ratios of 1:1.5, is a useful precursors for fabrication of silicon rich oxides. Annealing of this precursors at high temperature in slightly reducing conditions (4% H_2:96% Ar) delivers nc-Si in a silica matrix.

Polysiloxane nanofibres fabricated by methods presented in this thesis are of similar composition to HSQ. It is reasonable by way of some structural tailoring that fibres processed under similar conditions used for HSQ could be transformed into nc-Si/SiO_2 composite nanofibres.

However, before polysiloxane nanofibres can be used as precursors for SRO, any organic functionality must be removed from the polysiloxane network because, under reducing conditions, the Si-C bond stays intact.[130,135] This alone could impede the formation nc-Si/SiO_2. One possible solution to this problem is the synthesis of polysiloxane nanofibres using $HSiCl_3$ as the trichlorosilane precursor. Although fabrication of $HSiCl_3$ fibres may seem trivial, the substantial difference in volatility between $HSiCl_3$ and VTS requires an investigation into the optimal parameters for encouraging the formation of nanofibres over a thin film. If fabrication attempts are successful, this method offers the potential of providing

a technically rudimentary, cost effective fabrication of SRO with processing times < 24h.

5.3 Hierarchical Structure: Dry Adhesives

Geckos have the ability to scale walls and skirt across water because of unique structures on the pads of their feet which are comprised of microscopic bundles of flexible fibres (setae) subdivided into tiny spatula ranging from 200 – 500 nm in diameter. Each individual spatula interacts with a substrate via van der Waal forces[138,139] and the combined effect of all the fibres results in the unique phenomenon observed. Contact mechanic studies of these structures have shown that the adhesion force observed is proportional to the density of setae.[139] Other animals having similar adhesive abilities, *e.g.,* flies, have much larger attachment structures than the gecko.[139] Additionally, researchers have discovered that elastic modulus, E, of the β-keratinous fibres is much smaller than values obtained for bulk β-kerati[140,141] which enables the fibres to conform to surface roughness by a larger number of setae contacting the surface. Gecko's setae are also extremely hydrophobic in the non-bound state; a property which is thought to keep setae free of contamination that would interfere with the setae making contact with a surface during adhesion.[142] Based upon these detailed studies of the Gecko, it has been suggested that to mimic the gecko behaviour for the purpose of dry adhesives, a hierarchical structure of flexible nano-scale fibres superimposed on a micron sized features is required.[141] Additionally, hydrophobic fibres might be less prone to contamination through self-cleaning, and therefore potentially more durable.

Additionally, control of the fibre spatial density will provide materials with a range of adhesion.

The polysiloxanes fabricated in this work show great potential for use in adhesives mimicking the gecko architecture on account of the high spatial density achieved and hydrophobicity exhibited. To achieve a hierarchical structure, standard microfabrication techniques[37,40,143] could be utilized to produce the microfibres of appropriate dimensions (~30-130 μm long x ~10 μm in diameter) before functionalization with polysiloxane nanofibres. Additionally, the potentially tuneable flexibility of the polysiloxanes by the addition of R_2SiCl_2 to the reaction chamber (*vide supra*) would permit the fibre to more closely resemble the gecko with respect to the elastic modulus. By decreasing the spatial density of the polysiloxane fibres on the microstructure, the adhesion capability could also be controlled and customized to fit a specific application.

5.4 Conclusions

A reproducible method for the fabrication of poly(vinylsiloxane) nanofibres has been developed and the mechanism of formation has been proposed. Previous to this work, only two other research groups have published fabrication procedures for polysiloxane fibres < 100 nm and neither group have proposed a mechanism for fibre formation. Not only have we developed a reproducible method for polysiloxane nanofibres, but we have also demonstrated the ability to control the length, spatial density and wettability of the fibres produced. We have also extended the scope of this synthetic procedure by successfully fabricating

superhydrophobic co-polymer VTS/FTS nanofibres. Further, we have solution functionalized calcined fibres with FTS and concomitantly imparted the substrate surface with superhydrophobic wetting behaviour characteristics.

In conducting this work, many more questions have arisen that require further investigations in this area. For example, it is not clear why the fibres form with such a narrow distribution of diameters. Still, establishing a reproducible method for nanofibre fabrication provides the opportunity to investigate polysiloxanes for use in composition and refractory materials, chromatographic stationary phases, catalytic supports, dry adhesive, and silicon rich oxides. This method also provides a way of imparting surfaces with increased surface area and functionality while being relatively straightforward and technically straightforward. Although the procedure is not suitable for every application, it is another tool in the hypothetical toolbox for altering a material's surface chemistry.

5.5 References

1. *Silicon-Based Polymer Sicence A Comprehensive Resource*; Zeigler, J. M.; Fearon, G. F. W., Eds.; American Chemical Society: Washington, DC, 1990.
2. Mark, J. E.; Allcock, H. R.; West, R. *Inorganic Polymers*; 2nd ed.; Oxford University Press: New York, 2005.
3. *Synthesis and Properties of Silicones and Silicone-Modified Materials*; Clarson, S. J.; Fitzgerald, J. J.; Owen, M. J.; Smith, S. D.; Van Dyke, M. E., Eds.; American Chemical Society: Washington, DC, 2003.
4. Bausch, G. G.; Stasser, J. L.; Tonge, J. S.; Owen, M. J. *Plasmas Polym.* **1998**, *3*, 23-34.
5. Gao, L.; McCarthy, T. J. *Langmuir* **2006**, *2006*, 2966-2967.
6. Gao, L.; McCarthy, T. J. *J. Am. Chem. Soc.* **2006**, *128*, 9052-9053.
7. Kim, H. W.; Chung, C. W.; Rhee, Y. H. *Int. J. Biol. Macromol.* **2005**, *35*, 47-53.
8. Tsoi, S.; Fok, E.; Sit, J. C.; Veinot, J. G. C. *Langmuir* **2004**, *20*, 10771-10774.

9. Blodgett, K. B. *J. Am. Chem. Soc.* **1934**, *56*, 495-495.
10. Nuzzo, R. G.; Allara, D. L. *J. Am. Chem. Soc.* **1983**, *105*, 4481-4483.
11. Porter, M. D.; Bright, T. B.; Allara, D. L.; Chidsey, C. E. D. *J. Am. Chem. Soc.* **1987**, *109*, 3559-3568.
12. Troughton, E. B.; Bain, C. D.; Whitesides, G. M.; Nuzzo, R. G.; Allara, D. L.; Porter, M. D. *Langmuir* **1988**, *4*, 365-385.
13. Finklea, H. O.; Robinson, L. R.; Blackburn, A.; Richter, B.; Allara, D.; Bright, T. *Langmuir* **1986**, *2*, 239-244.
14. Kessel, C. R.; Granick, S. *Langmuir* **1991**, *7*, 532-538.
15. Carson, G.; Granick, S. *J. Appl. Polym. Sci.* **1989**, *37*, 2767-2772.
16. Sagiv, J. *J. Am. Chem. Soc.* **1980**, *102*, 92-98.
17. Wasserman, S. R.; Tao, Y. T.; Whitesides, G. M. *Langmuir* **1989**, *5*, 1074-1087.
18. Wenzel, R., N. *Ind. Eng. Chem.* **1936**, *28*, 988-994.
19. Hoffmann, P. W.; Stelzle, M.; Rabolt, J. F. *Langmuir* **1997**, *13*, 1877-1880.
20. Onclin, S.; Ravoo, B. J.; Reinhoudt, D. N. *Angew. Chem. Int. Ed.* **2005**, *44*, 6282-6304.
21. McGovern, M. E.; Kallury, K. M. R.; Thompson, M. *Langmuir* **1994**, *10*, 3607-3614.
22. Le Grange, J. D.; Markham, J. L.; Kurkjian, C. R. *Langmuir* **1993**, *9*, 1749-1753.
23. Silberzan, P.; Leger, L.; Ausserre, D.; Benattar, J. J. *Langmuir* **1991**, *7*, 1647-1651.
24. Bierbaum, K.; Grunze, M.; Baski, A. A.; Chi, L. F.; Schrepp, W.; Fuchs, H. *Langmuir* **1995**, *11*, 2143-2150.
25. Bunker, B. C.; Carpick, R. W.; Assink, R. A.; Thomas, M. L.; Hankins, M. G.; Voigt, J. A.; Sipola, D.; De Boer, M. P.; Gulley, G. L. *Langmuir* **2000**, *16*, 7742-7751.
26. Edmondson, S.; Osborne, V. L.; Huch, W. T. S. *Chem. Soc. Rev.* **2004**, *33*, 14-22.
27. Barthlott, W.; Neinhuis, C. *Planta* **1997**, *202*, 1-8.
28. Cassie, A. B. D.; Baxter, S. *Trans. Faraday. Soc.* **1944**, *40*, 546-551.
29. Larmour, I. A.; Bell, S. E. J.; Saunders, G. C. *Angew. Chem. Int. Ed.* **2007**, *46*, 1710-1712.
30. Shi, F.; Chen, X.; Wang, L.; Niu, J.; Yu, J.; Wang, Z.; Zhang, X. *Chem. Mater.* **2005**, *17*, 6177-6180.
31. Wang, M. F.; Raghunathan, N.; Ziaie, B. *Langmuir* **2007**, *23*, 2300-2303.
32. Ma, M.; Hill, R. M.; Lowery, J. L.; Fridrikh, S. V.; Rutledge, G. C. *Langmuir* **2005**, *21*, 5549-5554.
33. Woodward, I.; Schofield, W. C. E.; Roucoules, V.; Badya, J. P. S. *Langmuir* **2003**, *19*, 3432-3438.
34. Shibuichi, S.; Onda, T.; Satoh, N.; Tsujii, K. *J. Phys. Chem.* **1996**, *100*, 19512-19517.
35. Guo, Z.-G.; Fang, J.; Hao, J.-c.; Liang, Y.-m.; Liu, W.-m. *ChemPhysChem* **2006**, *7*, 1674-1677.

36. Shirtcliffe, N. J.; McHale, G.; Newton, M. I.; Perry, C. C.; Pyatt, F. B. *Appl. Phys. Lett.* **2006**, *89*, 104106-2.
37. Zhu, L.; Feng, Y.; Ye, X.; Zhou, Z. *Sensors and Actuators, A: Physical* **2006**, *130-131*, 595-600.
38. Martines, E.; Seunarine, K.; Morgan, H.; Gadegaard, N.; Wilkinson, C. D. W.; Riehle, M. O. *Nano Letters* **2005**, *5*, 2097-2103.
39. Extrand, C. W. *Langmuir* **2002**, *18*, 7991-7999.
40. Öner, D.; McCarthy, T. J. *Langmuir* **2000**, *16*, 7777-7782.
41. Tsoi, S.; Fok, E.; Sit, J. C.; Veinot, J. G. C. *Chem. Mater.* **2006**, *18*, 5260-5266.
42. Xu, J.; Li, M.; Zhao, Y.; Lu, Q. *Colloids Surf., A* **2007**, *302*, 136-140.
43. Li, Y.; Cai, W.; Cao, B.; Duan, G.; Sun, F.; Li, C.; Jia, L. *Nanotechnology* **2006**, *17*, 238-243.
44. Patankar, N. A. *Langmuir* **2004**, *20*, 8209-8213.
45. Huang, M. H.; Mao, S.; Feick, H.; Yan, H.; Wu, Y.; Kind, H.; Weber, E.; Russo, R.; Yang, P. *Science* **2001**, *292*, 1897-1900.
46. Xia, Y.; Yang, P.; Sun, Y.; Wu, Y.; Kim, F.; Yan, H. *Adv. Mater.* **2003**, *15*, 353-389.
47. Arnold, M. S.; Avouris, P.; Wei Pan, Z.; Wang, Z. L. *Journal of Physical Chemistry B.* **2002**, *107*, 659-663.
48. Cui, Y.; Lieber, C. M. *Science* **2001**, *291*, 851-854.
49. Cui, Y.; Wei, Q.; Park, H.; Lieber, C. M. *Science* **2001**, *293*, 1289-1293.
50. Jang, J.; Chang, M.; Yoon, H. *Adv. Mater.* **2005**, *17*, 1616-1620.
51. Virji, S.; Huang, J.; Kaner, R. B.; Weiller, B. H. *Nano Lett.* **2004**, *4*, 491-496.
52. Yu, D. P.; Hang, Q. L.; Ding, Y.; Zhang, H. Z.; Bai, Z. G.; Wang, J. J.; Zou, Y. H.; Zian, W.; Xiong, G. C.; Feng, S. Q. *Appl. Phys. Lett.* **1998**, *73*, 3076-3078.
53. Zheng, B.; Wu, Y.; Yang, P.; Liu, J. *Adv. Mater. (Weinheim, Fed. Repub. Ger.)* **2002**, *14*, 122-124.
54. Carter, J. D.; Qu, Y.; Porter, R.; Hoang, L.; Masiel, D. J.; Guo, T. *Chemical Communications* **2005**, 2274-2276.
55. Hu, J. Q.; Jiang, Y.; Meng, X. M.; Lee, C. S.; Lee, S. T. *Chem. Phys. Lett.* **2003**, *367*, 339-343.
56. Verheijen, M. A.; Immink, G.; de Smet, T.; Borgstrom, M. T.; Bakkers, E. P. A. M. *J. Am. Chem. Soc.* **2006**, *128*, 1353-1359.
57. Wang, X.; Ding, Y.; Summers, C. J.; Wang, Z. L. *J. Phys. Chem. B* **2004**, *108*, 8773-8777.
58. Jang, J.; Bae, J.; Park, E. *Adv. Funct. Mat.* **2006**, *16*, 1400-1406.
59. Zhang, M.; Bando, K.; Wada, K.; Kurashima, K. *J. Mater. Sci. Lett.* **1999**, *18*, 1911-1913.
60. Yu, T.; Joo, J.; Park, Y. I.; Hyeon, T. *J. Am. Chem. Soc.* **2006**, *128*, 1786-1787.
61. Li, D.; Xia, Y. *Nano Lett.* **2003**, *3*, 555-560.

62. Deitzel, J. M.; Kleinmeyer, J. D.; Hirvonen, J. K.; Tan, N. C. B. *Polymer* **2001**, *42*, 8163-8170.
63. Doshi, J.; Reneker, D. H. *Journal of Electrostatics* **1995**, *35*, 151-160.
64. Kameoka, J.; Verbridge, S. S.; Jiu, H.; Czaplewski, D. A.; Craighead, H. G. *Nano Lett.* **2004**, *4*, 2105-2108.
65. Jeong, H. E.; Lee, S. H.; Kim, P.; Suh, K. Y. *Nano Lett.* **2006**, *6*, 1508-1513.
66. Abu-Lail, N. I.; Kaholek, M.; LaMattina, B.; Clarck, R. L.; Zauscher, S. *Sensors and Actuators B* **2006**, *114*, 371-378.
67. Kim, J. W.; Chung, C. W.; Rhee, Y. H. *International Journal of Biological Macromolecules* **2005**, *35*, 47-53.
68. Bae, J.-S.; Seo, E.-J.; Kang, I.-K. *Biomaterials* **1999**, *20*, 529-537.
69. Seino, M.; Yokomachi, K.; Hayakawa, T.; Kikuchi, R.; Kakimoto, M.-a.; Horiuchi, S. *Polymer* **2006**, *47*, 1946-1952.
70. Gupta, B.; Hilborn, J. G.; Bisson, I.; Frey, P. *J. Appl. Polym. Sci.* **2001**, *81*, 2993-3001.
71. Gupta, B.; Anjum, N. *Adv. Polym. Sci.* **2003**, *162*, 36-61.
72. Bae, B.; Ha, Y. H.; Kim, D. *Journal of Membrane Science* **2006**, *276*, 51-58.
73. Zhong, S.; Meng, Y.; OU, Q.; Shu, Z. *Plasma Science & Technology* **2006**, *8*, 321-324.
74. Nguyen, V.; Yoshida, W.; Cohen, Y. *J. Appl. Polym. Sci.* **2003**, *87*, 300-310.
75. Sagiv, J. *J. Am. Chem. Soc.* **1980**, *102*, 92-98.
76. Popat, K. C.; Johnson, R. W.; Desai, T. A. *Surface and Coatings Technology* **2002**, *154*, 253-261.
77. Bunker, B. C.; Carpick, R. W.; Assink, R. A.; Thomas, M. L.; Hankins, M. G.; Voigt, J. A.; Sipola, D.; de Boer, M. P.; Gulley, G. L. *Langmuir* **2000**, *16*, 7742-7751.
78. Wasserman, S. R.; Tao, Y.-T.; Whitesides, G. M. *Langmuir* **1989**, *5*, 1074-1087.
79. Yoshida, W.; Castro, R. P.; Jou, J.-D.; Cohen, Y. *Langmuir* **2001**, *17*, 5882-5888.
80. Tsoi, S.; Fok, E.; Sit, J. C.; Veinot, J. G. C. *Langmuir* **2004**, *20*, 10771-10774.
81. Wang, Y.; Ferrari, M. *J. Mat. Sci* **2000**, *35*, 4923-4930.
82. Schwartz, D. K.; Steinberg, S.; Israelachvili, J.; Zasadzinski, J. A. N. *Phys. Rev. Lett.* **1992**, *69*, 3354-3357.
83. Popat, K.; Sharma, S.; Johnson, R. W.; Desai, T. A. *Surf. Interface Anal.* **2003**, *35*, 205-215.
84. No effort was made to free the reaction chamber of surface adsorbed water.
85. Silberzan, P.; Léger, L.; Ausserré, D.; Benattar, J. J. *Langmuir* **1991**, *7*, 1647-1651.
86. Cassie, A. B. D.; Baxter, S. *Transcations of Faraday Society* **1944**, *40*, 546-551.

87. Bico, J.; Thiele, U.; Quéré, D. *Colloids and Surfaces A: Physicochem. Eng. Aspects* **2002**, *2006*, 41-46.
88. Brunner, H.; Vallant, T.; Mayer, U.; Hoffmann, H. *Langmuir* **1999**, *15*, 1899-1901.
89. Finklea, H. O.; Robinson, L. R.; Blackburn, A.; Richter, B. *Langmuir* **1986**, *2*, 239-244.
90. Senaratne, W.; Andruzzi, L.; Ober, C. K. *Biomacromolecules* **2005**, *6*, 2427-2448.
91. Williams, K. R.; Gupta, K.; Wasilik, M. *J. Microelectromech. Syst.* **2003**, *12*, 761-778.
92. Kern, W. *J. Electrochem. Soc.* **1990**, *137*, 1887-1892.
93. Rollings, D. E.; Tsoi, S.; Sit, J. C.; Veinot, J. G. C. *Langmuir* **2007**, *23*, 5275-5278.
94. Kern, W. *Handbook of Semiconductor Wafer Cleaning Technology - Science, Technology, and Applications*; William Andrew Publishing/Noyes: New Jersey, 1993.
95. Mun, S. Y.; Jang, Y. S.; Ko, Y. S.; Huh, S. B.; Lee, J. K.; Jeong, Y. H. *J. Electrochem. Soc.* **2006**, *153*, G866-G869.
96. Sirghi, L.; Kylian, O.; Gilliland, D.; Ceccone, G.; Rossi, F. *J. Phys. Chem. B* **2006**, *110*, 25975-25981.
97. Artus, G. R. J.; Jung, S.; Zimmermann, J.; Gautschi, H. P.; Marquardt, K.; Seeger, S. *Adv. Mater.* **2006**, *18*, 2758-2762.
98. Dong, J.; Wang, A.; Ng, K. Y. S.; Mao, G. *Thin Solid Films* **2006**, *515*, 2116-2122.
99. Jorgensen, W. L.; Maxwell, D. S.; Tirado-Rives, J. *J. Am. Chem. Soc.* **1996**, *118*, 11225-11236.
100. Stevens, M. J. *Langmuir* **1999**, *15*, 2773-2778.
101. Rye, R. R.; Nelson, G. C.; Dugger, M. T. *Langmuir* **1997**, *13*, 2965-2972.
102. Rye, R. R. *Langmuir* **1997**, *13*, 2588-2590.
103. Gao, L.; McCarthy, T. J. *Langmuir* **2007**, *23*, 3762-3765.
104. Lafuna, A.; Quéré, D. *Nature Materials* **2003**, *2*, 457-460.
105. Extrand, C. W. *Langmuir* **2003**, *19*, 3793-3796.
106. Bartell, F. E.; Shepard, J. W. *J. Phys. Chem.* **1953**, *57*, 455.
107. Swain, P. S.; Lipowsky, R. *Langmuir* **1998**, *14*, 6772-6780.
108. Chen, W.; Fadeev, A. Y.; Zhsieh, M. C.; Öner, D.; Youngblood, J.; McCarthy, T. J. *Langmuir* **1999**, *15*, 3395-3399.
109. Mansky, P.; Lui, Y.; Huang, E.; Russell, T. P.; Hawker, C. *Science* **1997**, *275*, 1458-1460.
110. Zhu, L.; Xiu, Y.; Xu, J.; Tamirisa, P. A.; Hess, D. W.; Wong, C.-P. *Langmuir* **2005**, *21*, 11208-11212.
111. Sneh, O.; George, S. M. *J. Phys. Chem.* **1995**, *99*, 4639-4647.
112. Solomons, T. W. G.; Fryhle, C. B. *Organic Chemistry*; 9th ed.; John Wiley: Hoboken, 2008.
113. Levkin, P. A.; Ruderisch, A.; Schurig, V. *Chirality* **2006**, *18*, 49-63.

114. Del Zotto, A.; Greco, C.; Baratta, W.; Siega, K.; Rigo, P. *Eur. J. Inorg. Chem.* **2007**, 2909-2916.
115. *Advances in Silicon Carbide Processing and Applications*; Saddow, S. E.; Agarwal, A. K., Eds.; Artech House: Boston, 2004.
116. Ryu, Y.; Tak, Y.; Yong, K. *Nanotechnology* **2005**, *16*, S370-S374.
117. Onat, A.; Akbulut, H.; Yilmaz, F. *J. Alloys Compd.* **2007**, *436*, 375-382.
118. Wong, E. W.; Sheehan, P. E.; Lieber, C. M. *Science* **1997**, *277*, 1971-1975.
119. Schubert, U.; Hüsing, N. In *Synthesis of Inorganic Materials*; Wiley-VCH: Weinheim, 2000, p 18-21.
120. Wu, R. B.; Yang, G. Y.; Pan, Y.; Chen, J. J. *J. Mater. Sci.* **2007**, *42*, 3800-3804.
121. Dai, H.; Wong, E. W.; Lu, Y. Z.; Fan, S.; Lieber, C. M. *Nature* **1995**, *375*, 769-772.
122. Gao, Y. H.; Bando, Y.; Kurashima, K.; Sato, T. *J. Mater. Sci.* **2002**, *37*, 2023-2029.
123. Meng, G. W.; Zhang, L. D.; Mo, C. M.; Zhang, S. Y.; Qin, Y.; Feng, S. P.; Li, H. J. *Solid State Commun.* **1998**, *106*, 215-219.
124. Yang, Z.; Xia, Y.; Mokaya, R. *Chem. Mater.* **2004**, *16*, 3877-3884.
125. Lai, H. L.; Wong, N. B.; Zhou, X. T.; Peng, H. Y.; Au, F. C. K.; Wang, N.; Bello, I.; Lee, C. S.; Lee, S. T.; Duan, X. F. *Appl. Phys. Lett.* **2000**, *76*, 294-296.
126. Wei, J.; Li, K. Z.; Li, H. J.; Fu, Q. G.; Zhang, L. *Mater. Chem. Phys.* **2006**, *95*, 140-144.
127. Huczko, A.; Bystrzejewski, M.; Lange, H.; Fabianowska, A.; Cudzilo, S.; Panas, A.; Szala, M. *J. Phys. Chem. B* **2005**, *109*, 16244-16251.
128. Hao, Y. J.; Jin, G. Q.; Han, X. D.; Guo, X. Y. *Mater. Lett.* **2006**, *60*, 1334-1337.
129. Liu, X.-M.; Yao, K.-F. *Nanotechnology* **2005**, *16*, 2932-2935.
130. Richter, R.; Roewer, G.; Bohme, U.; Busch, K.; Babonneau, F.; Martin, H. P.; Muller, E. *Appl. Organomet. Chem.* **1997**, *11*, 71-106.
131. Interrante, L. V.; Moraes, K.; Liu, Q.; Lu, N.; Puerta, A.; Sneddon, L. G. *Pure Appl. Chem.* **2003**, *74*, 2111-2117.
132. Yang, W.; Miao, H.; Xie, Z.; Zhang, L.; An, L. *Chem. Phys. Lett.* **2004**, *383*, 441-444.
133. Cai, K. F.; Lei, Q.; Zhang, L. C. *Journal of Nanoscience and Nanotechnology* **2005**, *5*, 1925-1928.
134. Brunner, A. R.; Bujalski, D. R.; Moyer, E. S.; Su, K.; Sneddon, L. G. *Chem. Mater.* **2000**, *12*, 2770-2780.
135. Raman, V.; Bhatia, G.; Mishra, A. K.; Bhardwaj, S.; Sood, K. N. *Mater. Lett.* **2006**, *60*, 3906-3911.
136. Yang, Z. X.; Jun, Y. J.; Zhu, F.; Zhang, Y. *Physica E: Low-Dimensional Systems and Nanostructures* **2005**, *25*, 395-398.
137. Hessel, C. M.; Henderson, E. J.; Veinot, J. G. C. *Chem. Mater.* **2006**, *18*, 6139-6146.

138. Autumn, K.; Sitti, M.; Liang, Y. A.; Peattie, A. M.; Hansen, W. R.; Sponberg, S.; Kenny, T. W.; Fearing, R.; Israelachvili, J. N.; Full, R. J. *PNAS* **2002**, *99*, 12252-12256.
139. Arzt, E.; Gorb, S.; Spolenak, R. *PNAS* **2003**, *100*, 10603-10606.
140. Autumn, K.; Majidi, C.; Groff, R. E.; Dittmore, A.; Fearing, R. *J. Exp. Biol.* **2006**, *209*, 3558-3568.
141. Persson, B. N. J. *J. Chem. Phys.* **2003**, *118*, 7614-7621.
142. Autumn, K.; Hansen, W. *Journal of Comparative Physiology A: Neuroethology, Sensory, Neural, and Behavioral Physiology* **2006**, *192*, 1205-1212.
143. Xia, Y.; Whitesides, G. M. *Angew. Chem. Int. Ed.* **1998**, *37*, 550-575.

Appendices

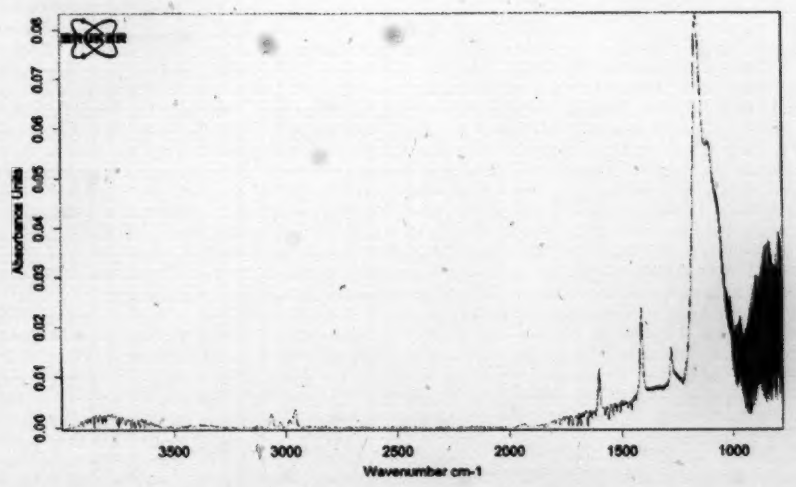

Figure A1- 1.. Variable angle FTIR of VTS fibres on Si substrate taken with Si background. Angle was set to 75° to the surface with 90° polarization of beam.

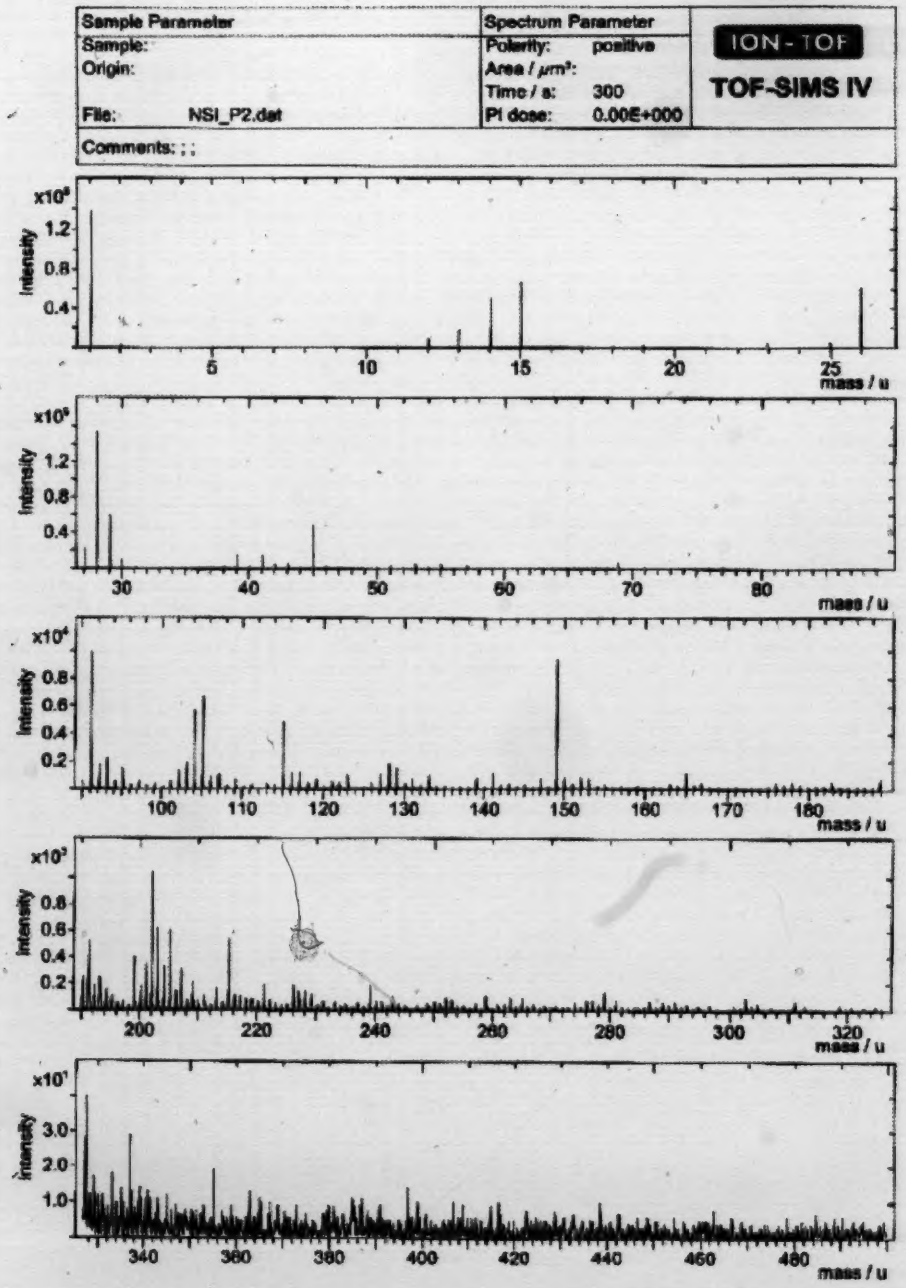

Figure A1- 2. Positive polarity TOF-SIMS spectrum of VTS fibres prepared on Si substrates.

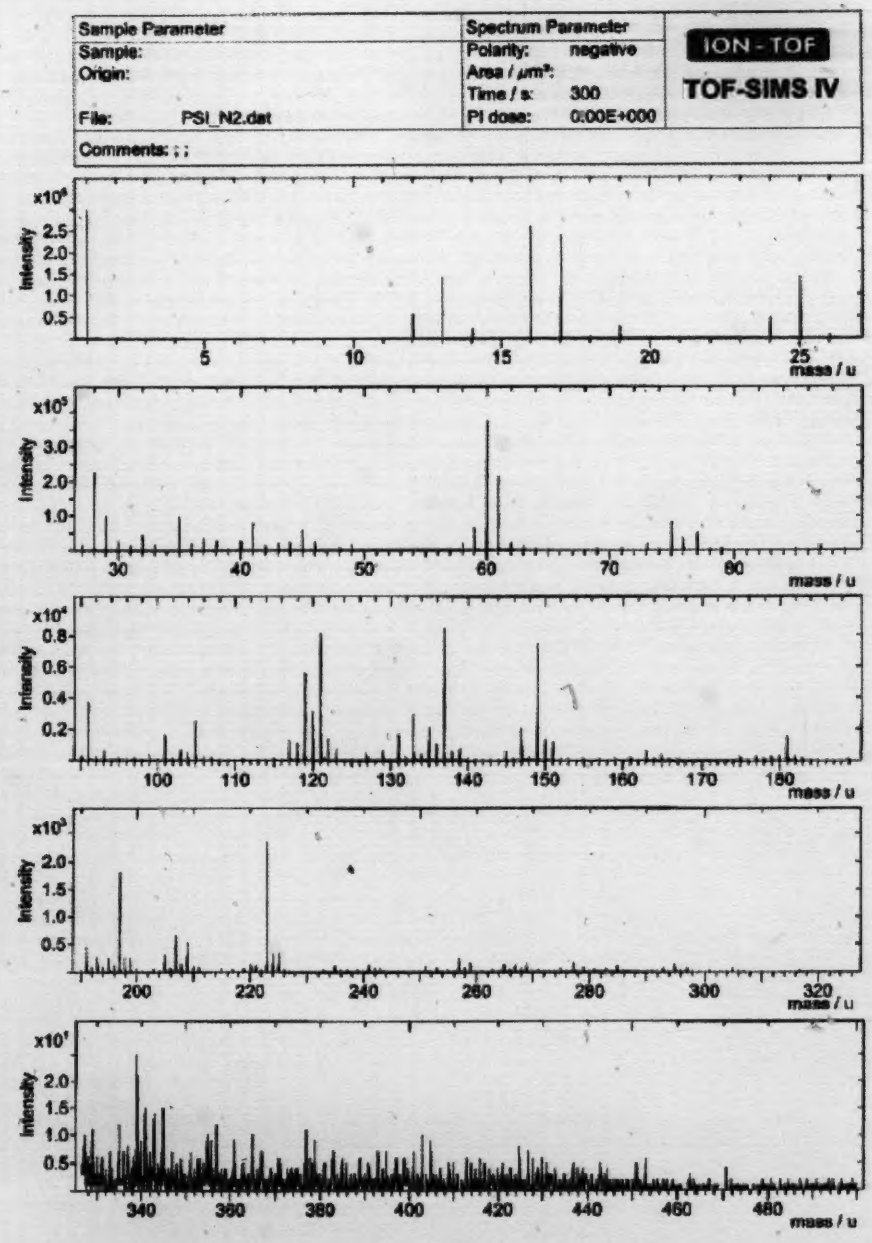

Figure A1- 3. Negative polarity TOF-SIMS spectrum of VTS fibres prepared on Si substrates.

Table A1- 1. Positively and negatively charged fragments with mass/charge ratios corresponding to TOF-SIMS spectra presented above.

m/e⁻	fragment
15	$^{3+}$SiOH
45	

m/e⁻	fragment
17	⁻OH
25	
60	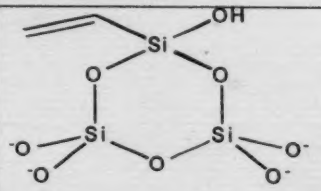
61	
121	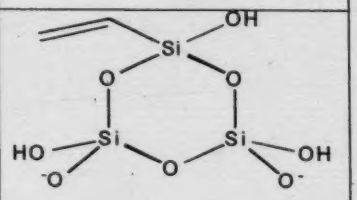

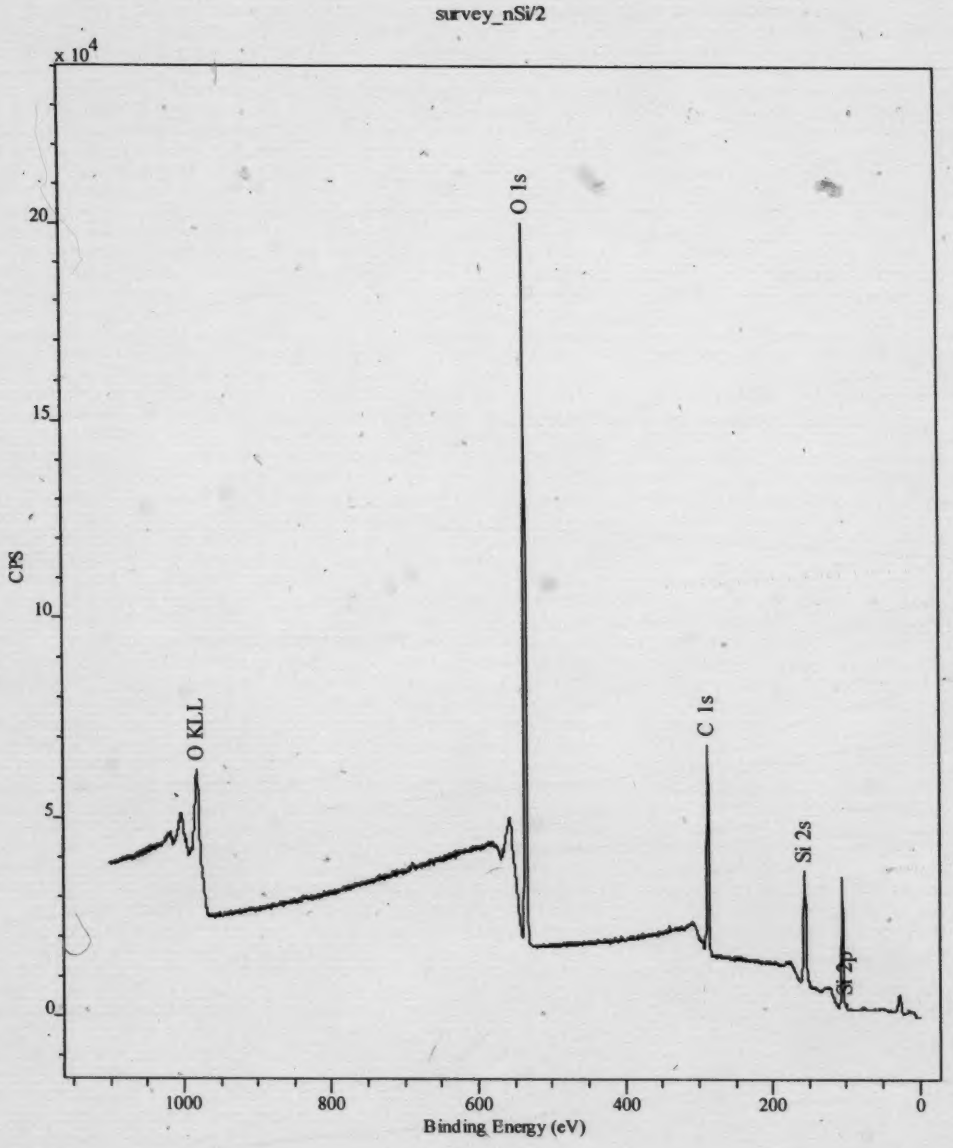

Figure A1- 4 Survey XPS of VTS fibres clearly identifying the presence of carbon, silicon and oxygen as well as the absence of chlorine.

Figure A1- 5. SEM image of substrate exposed to butyltrichlorosilane. Scale bar is 500 nm.

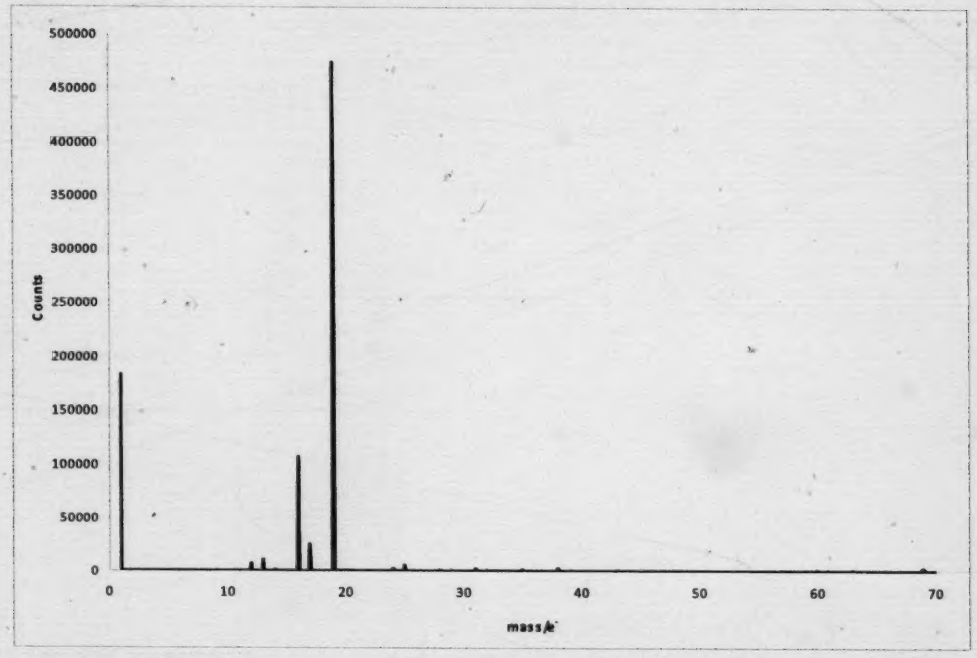

Figure A1- 6. Negative ToF-SIMS spectrum of calcined fibres functionalized with FTS.